MINISTRY OF EDUCATION AND RESEARCH

UNIVERSITAS GALATIENSIS

UNIVERSITAS GALATIENSIS FACULTATEA DE INGINERIE

# THE ANNALS OF “DUNAREA DE JOS” UNIVERSITY OF GALATI

## Fascicle IX
## METALLURGY AND MATERIALS SCIENCE

YEAR XLIII (XLVIII)
March 2025, no. 1

ISSN 2668-4748; e-ISSN 2668-4756

GALATI UNIVERSITY PRESS

2025

THE ANNALS OF "DUNAREA DE JOS" UNIVERSITY OF GALATI
FASCICLE IX. METALLURGY AND MATERIALS SCIENCE
N°. 1 - 2025, ISSN 2668-4748; e-ISSN 2668-4756
Volume DOI: https://doi.org/10.35219/mms.2025.1

# Table of Contents

THE ANNALS OF "DUNAREA DE JOS" UNIVERSITY OF GALATI
FASCICLE IX. METALLURGY AND MATERIALS SCIENCE
N°. 1 - 2025, ISSN 2668-4748; e-ISSN 2668-4756
Article DOI: https://doi.org/10.35219/mms.2025.1.01

# SOME ASPECTS REGARDING THE ACTION OF VIBRATIONS ON THE HUMAN KNEE JOINT

**Marina Gabriela DOGARU, Cristian PAVEL**
Faculty of Mechanical Engineering and Robotics in Construction-U.T.C.B., Romania
e-mail: marina.dogaru78@gmail.com, cpcristianpavel@gmail.com

## ABSTRACT

*Machines that use vibrations in the work process are found in various activities, on construction sites or within the premises of some constructions. Their operators are affected over time by mechanical oscillations. Entering the body through the hand-arm assembly, through the legs, or while sitting, the vibrations affect the human body, usually in a negative way. The positive effects are currently being studied in order to be able to improve various human joint conditions or to improve physical condition, but exposure must be done in a controlled environment and under well-established conditions defined by specialists.*

*Over time, various studies have been carried out and solutions have been sought to reduce the effects of vibrations on the human body. The difficulty of performing in vivo experiments on people has led to the use of increasingly complex theoretical models to study the problem. By comparing the results obtained from modeling with experimental results collected through measurements under different conditions on the construction site or in the laboratory, useful information was obtained, which can be used to improve the working conditions of workers.*

*The search for a theoretical model as efficient as possible, and for methods as fast as possible to obtain information about the vibrations that affect the human body, is ongoing, the human body being very complex and difficult to model.*

*This article investigates the effect of mechanical oscillations on the knee joint of rotary hammer operators, comparing results obtained through laboratory measurements with those obtained from modeling.*

KEYWORDS: mechanical oscillations, rotary impact machine, knee joint

## 1. Introduction

A wide variety of rotary hammer machines are used both on open-air organized construction sites and within the premises of new constructions or those that are being rehabilitated. Their excessive use can produce vibrations with harmful effects on the bodies of their operators.

Oscillatory movements enter the human body through the hand-arm system, while sitting, or through the legs.

Each individual responds differently to the influence of vibrations. Among the relevant factors tare: age, tolerance to oscillations, state of health, etc.

Research conducted over time has shown that the internal organs of the human body have their own natural oscillation frequencies, and the effect of vibrations on the human body can be amplified due to resonance [1].

The lower limb, like the internal organs, can be affected by vibrations generated by the equipment used by humans. One of its joints, the human knee, is a complex joint that connects the thigh to the calf. It is a pivoting joint with the ability to bear weight [2]. Exposure to vibration affects this joint over time. Depending on the duration of exposure and the frequency of oscillations, there may also be some positive effects.

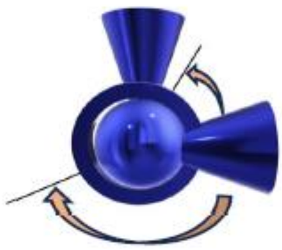

***Fig. 1.*** *The knee joint* [2, 5]

THE ANNALS OF "DUNAREA DE JOS" UNIVERSITY OF GALATI
FASCICLE IX. METALLURGY AND MATERIALS SCIENCE
N°. 1 - 2025, ISSN 2668-4748; e-ISSN 2668-4756
Article DOI: https://doi.org/10.35219/mms.2025.1.01

Studies conducted over time have mainly focused on the negative effects of vibrations and how to protect operators.

In papers [3] and [4], a 3D model with 12 degrees of freedom for the human knee was proposed for studying movement and analysing the forces acting on it [2].

Human gait and the effects of body weight on it were the subjects of research conducted by Anne E. Martin and James P. Schmiedeler in 2014 and by Stefan Seiterle, Tyler Susko, Panagiotis K. Artemiadis, Robert Riener, and Hermano Igo Krebs in 2015 [2].

A 2016 study on human fall risk by Anne E. Martin, Dario J. Villarreal and Robert D. Gregg led to the development of a kinematic model of the human knee that can be integrated into a complex gait model [2, 6].

Akio Yamamoto, Shun Sasagawa, Naoko Oba and Kimitaka Nakazawa (2015), as well as Hyunggwi Song, Heewon Park, and Sukyung Park (2016), presented pendulum-type models of the lower limb in their published works, designed to investigate human gait [2, 7, 8].

An article published in 2018 by Raj Desai, Anirban Guha, and P. Seshu, researchers at the Indian Institute of Technology Bombay, Department of Mechanical Engineering, presents a biomechanical model of a seated individual with 20 degrees of freedom. The model was created to study the effects of low-frequency vibrations on the human body during the operation of heavy machinery and various vehicles [2, 9].

Raynaud's syndrome, a condition resulting from exposure to vibrations in the upper and lower limbs, affects the vascular and neurological systems. This condition manifests as numbness, tingling, and whitening of the toes or fingers. The problem was studied by Goggins, Tarabini, et al. in 2019, who sought to identify the resonance frequencies of different areas of the human foot in a natural position. The same topic was also researched by D. Chadefaux et al. in 2020, whose results may lead to the development of new materials and improvements in equipment designed to attenuate vibrations transmitted through the feet [2, 10].

Vibrations can have beneficial effects on the knee joint and the human body under certain well-defined conditions. Studies conducted in recent years have followed this line of research, particularly in the medical field.

In order to reduce the negative effects of vibrations (typically through damping or isolation) it is first necessary to determine the levels of certain vibration characteristics.

The authors propose to measure, as accurately as possible, the level of vibrations acting on the operator's knee joint while using a rotary hammer.

***Fig. 2.*** *Rotary impact machine used to perforate various materials* [13]

## 2. Theoretical model

Reviewing the models presented in the literature, the authors considered it appropriate to study the effect of vibrations on the knee joint using a physical double pendulum model (Figure 3), in which the lower leg and foot are modeled as an articulated bar connected to a bar representing the thigh. Two disturbing forces, F_1 and F_2, were assumed to act on the double pendulum.

To dampen vibrations and limit displacement, two pairs of elastic springs were placed at the centres of gravity of the bars [2].

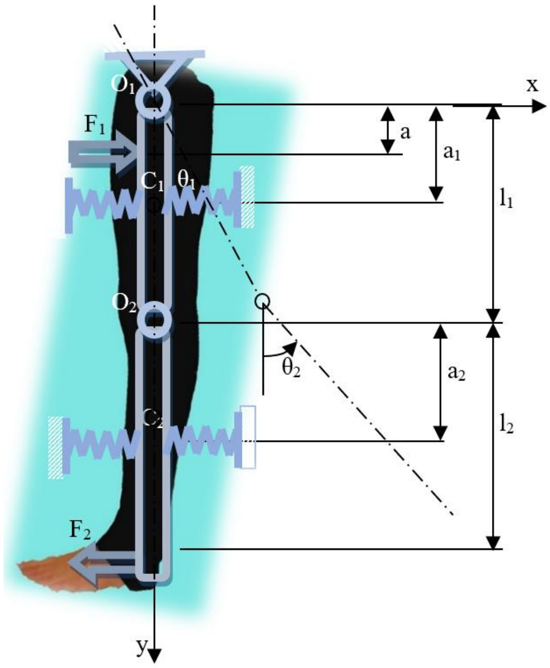


***Fig. 3.*** *Theoretical calculation model* [2]

In order to achieve the proposed goal -namely, the determination of the pulsations of the considered system and the application of real values in the study - Lagrange's equations of the second kind were used.

The differential equations of the mechanical system in Figure 3, in matrix form, are presented in equation (1). It should be noted that the notations used are identical to those commonly found in the specialized literature.

After performing the calculations, we obtained the equation of the natural pulsations, given in equation (2).

In order to solve the equation of the natural pulsations, we started from the following anthropometric data presented in Table 1.

The estimated values for the position of the centre of gravity for the thigh ($a_1$) is 21.65 cm, and for the calf and foot ($a_2$) is 23.81 cm. The hip and knee joints were denoted by $O_1$ and $O_2$; $C_1$ – the centre of gravity of the thigh; $C_2$ – the centre of gravity of the calf and foot.

Using dedicated vibration sensors, measurements were made on a single person operating a rotary hammer (the source of vibration). Data collection was performed by attaching the accelerometer, alternately, to the drill and to the knee of the person operating the tool. Tests were performed while the drill was running idle and then when it was being used to perform various operations.

The measurements were made with professional vibration sensors, typically used in demanding static situations scenarios.

The operator's anthropometric data were identical to those used in the calculation aimed at determining the intrinsic pulsations (see Table 1, Chapter 2).

$$\begin{bmatrix} \frac{m_1 l_1^2}{3} + m_2 l_1^2 & m_2 l_1 a_2 \\ m_2 l_1 a_2 & \frac{m_2 l_2^2}{12} + m_2 a_2^2 \end{bmatrix} \begin{Bmatrix} \ddot{\theta}_1 \\ \ddot{\theta}_2 \end{Bmatrix} + \begin{bmatrix} m_1 g a_1 + m_2 g l_1 + 2k_1 a_1^2 + 2k_2 l_1^2 & 2k_2 l_1 a_2 \\ 2k_2 l_1 a_2 & m_2 g a_2 + 2k_2 a_2^2 \end{bmatrix} \begin{Bmatrix} \theta_1 \\ \theta_2 \end{Bmatrix} = \begin{Bmatrix} F_{01} a \\ F_{02} l_2 \end{Bmatrix} sin\omega t \quad (1)$$

$$\left[(m_1 g a_1 + m_2 g l_1 + 2k_1 a_1^2 + 2k_2 l_1^2) - \left(\frac{m_1 l_1^2}{3} + m_2 l_1^2\right) \cdot p^2\right] \cdot \left[(m_2 g a_2 + 2k_2 a_2^2) - \left(\frac{m_2 l_2^2}{12} + m_2 a_2^2\right) \cdot p^2\right] - (2k_2 l_1 a_2 - m_2 l_1 a_2 p^2)^2 = 0 \quad (2)$$

***Table 1.*** *Anthropometric dimensions of the operator* [2]

| Total mass [kg] | Thigh mass [kg] | Calf mass [kg] | Foot mass [kg] | Calf and foot mass [kg] | Thigh height, l1 [m] | Calf height [m] | Foot height [m] | Calf and foot height, l2 [m] | Total height [m] | Leg length, $l_p$ [m] |
|---|---|---|---|---|---|---|---|---|---|---|
| 104 | 10.5 | 5.61 | 1.97 | 11.05 | 0.5 | 0.47 | 0.08 | 0.55 | 1.71 | 0.26 |

The estimates were made starting from the total mass of the individual and from the dimensions of the lower limb segments, according to [4].

After substituting the values presented above, the pulsation equation is obtained in the form:

$$(244.127 - 3.638 \cdot p^2) \cdot (55.431 - 0.863 \cdot p^2) - (66.302 - 1.271 \cdot p^2)^2 = 0$$

The values of the system's natural pulsations, obtained by solving the equation using Wolfram Alpha software, satisfying the specified conditions (positive values, see [4]), are: $p_1 = 7{,}74089\ s^{-1}$ and $p_2 = 10{,}0018\ s^{-1}$.

## 3. Experimental determinations

Within the Research Institute for Construction Equipment and Technologies - ICECON S.A., the necessary measurements for the experimental part of the study were performed.

The 4506-B-003 Brüel & Kjaer sensor was used for most tests. To improve sensitivity in data collection from the knee joint area, the HVA-4447 sensor was used.

***Fig. 4.*** *Sensors used for measurements* [2]

***Fig. 5.** The operator during the tests* [2]
*(images taken from a personal archive)*

Measurements were performed in a controlled environment, with the 4506-B-003 Brüel & Kjaer sensor mounted on the knee. Acceleration values and the Fast Fourier Transform response to the signal received from it are presented in Tables 2 and 3, and in Figures 6 and 7.

***Table 2.** Acceleration signal measured over time with 4506-B 003 Brüel&Kjaer* [2]

| axis x | | axis y | | axis z | |
|---|---|---|---|---|---|
| Time - Acceleration_0 | | Time - Acceleration_1 | | Time - Acceleration_2 | |
| 0 | 1.96864 | 0 | 1.53548 | 0 | 0.952996 |
| 0.0002 | 1.99453 | 0.0002 | 1.5684 | 0.0002 | 0.843923 |
| 0.0004 | 1.94018 | 0.0004 | 1.55931 | 0.0004 | 0.891622 |
| 0.0006 | 1.93933 | 0.0006 | 1.51778 | 0.0006 | 0.989659 |
| 0.0008 | 2.01936 | 0.0008 | 1.54625 | 0.0008 | 0.873572 |

***Table 3.** Frequency spectrum analysis for data collected by the sensor 4506-B 003 Brüel&Kjaer* [2]

| axis x<br>Frequency - Acceleration_0 (FFT - (RMS)) | | axis y<br>Frequency - Acceleration_1 (FFT - (RMS)) | | axis z<br>Frequency - Acceleration_2 (FFT - (RMS)) | |
|---|---|---|---|---|---|
| 28.3088 | 0.000375 | 28.3088 | 0.0037335 | 28.3088 | 0.0019797 |
| 28.3824 | 0.001598 | 28.3824 | 0.0034778 | 28.3824 | 0.0020299 |
| 28.4559 | 0.0014465 | 28.4559 | 0.003396 | 28.4559 | 0.0007455 |
| 28.5294 | 0.0011605 | 28.5294 | 0.0035702 | 28.5294 | 0.0018432 |
| 28.6029 | 0.0005488 | 28.6029 | 0.0037101 | 28.6029 | 0.0016722 |

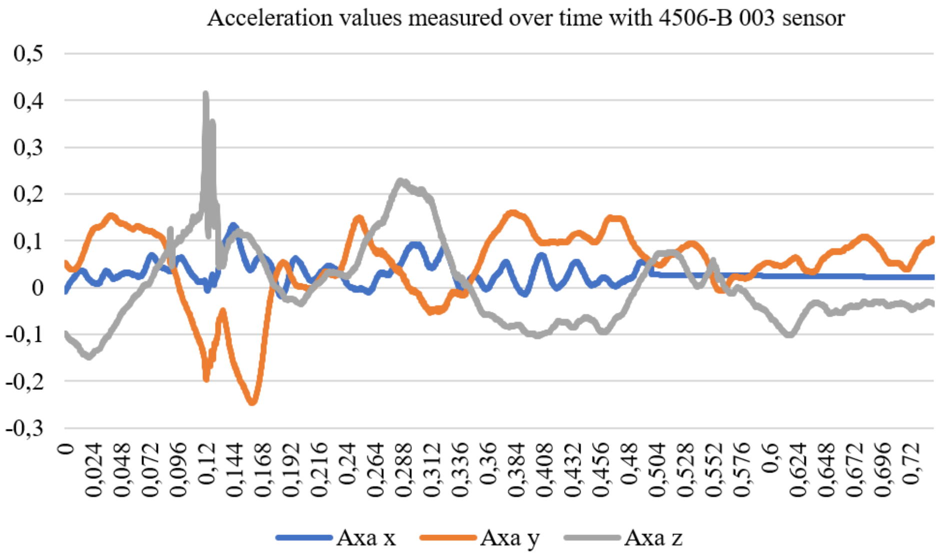


***Fig. 6.** Results obtained when measuring acceleration with the Brüel&Kjaer 4506-B 003 sensor located on the operator's knee*

N°. 1 - 2025, ISSN 2668-4748; e-ISSN 2668-4756
Article DOI: https://doi.org/10.35219/mms.2025.1.01

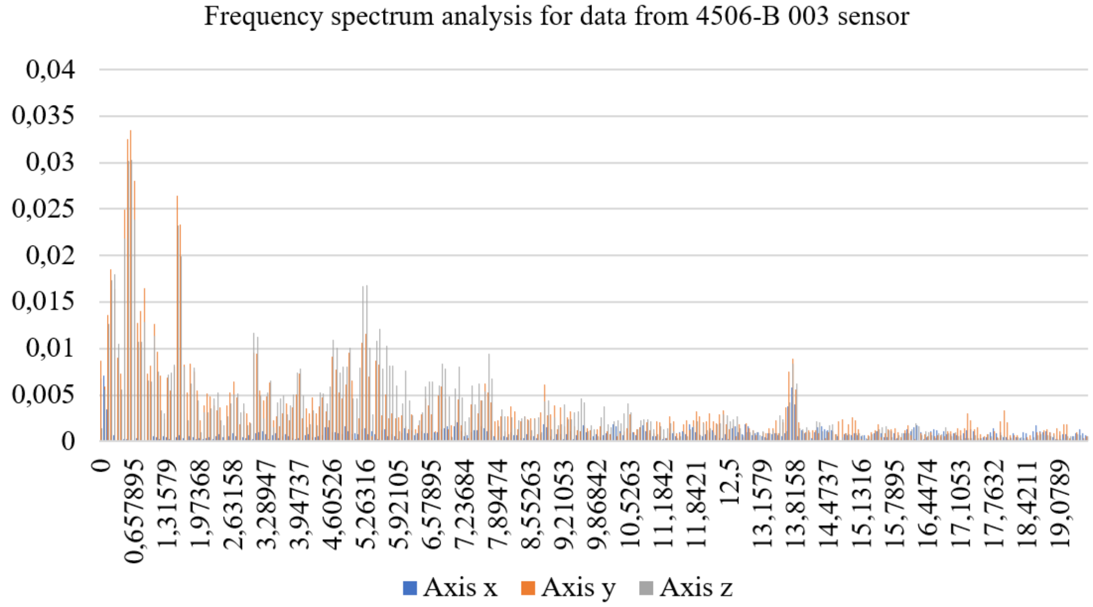


***Fig. 7.*** *Frequency spectrum analysis for data obtained with Brüel&Kjaer 4506-B 003 sensor*

***Table 4.*** *Acceleration signal measured over time with HVA 4447 sensor* [2]

| axis x | | axis y | | axis z | |
|---|---|---|---|---|---|
| Time - Acceleration_0 | | Time - Acceleration_1 | | Time - Acceleration_2 | |
| 0 | -0.0081065 | 0 | 0.0530285 | 0 | -0.0993299 |
| 0.0002 | -0.00726 | 0.0002 | 0.0528431 | 0.0002 | -0.0981359 |
| 0.0004 | -0.0061183 | 0.0004 | 0.0513116 | 0.0004 | -0.0997383 |
| 0.0006 | -0.0050573 | 0.0006 | 5.07E-02 | 0.0006 | -0.0986921 |
| 0.0008 | -0.0039561 | 0.0008 | 0.0508645 | 0.0008 | -0.100873 |

***Table 5.*** *Frequency spectrum analysis for data collected by the sensor HVA 4447* [2]

| axis x | | axis y | | axis z | |
|---|---|---|---|---|---|
| Frequency - Acceleration_0 (FFT - (RMS)) | | Frequency - Acceleration_1 (FFT - (RMS)) | | Frequency - Acceleration_2 (FFT - (RMS)) | |
| 28.1579 | 0.0003477 | 28.1579 | 0.0005003 | 28.1579 | 0.00157591 |
| 28.2237 | 0.0005421 | 28.2237 | 3.33E-04 | 28.2237 | 0.000648375 |
| 28.2895 | 0.000567 | 28.2895 | 0.0006668 | 28.2895 | 0.00149551 |
| 28.3553 | 0.0002332 | 28.3553 | 0.00072 | 28.3553 | 0.00193745 |
| 28.4211 | 1.20E-04 | 28.4211 | 4.32E-04 | 28.4211 | 0.000947946 |

N°. 1 - 2025, ISSN 2668-4748; e-ISSN 2668-4756
Article DOI: https://doi.org/10.35219/mms.2025.1.01

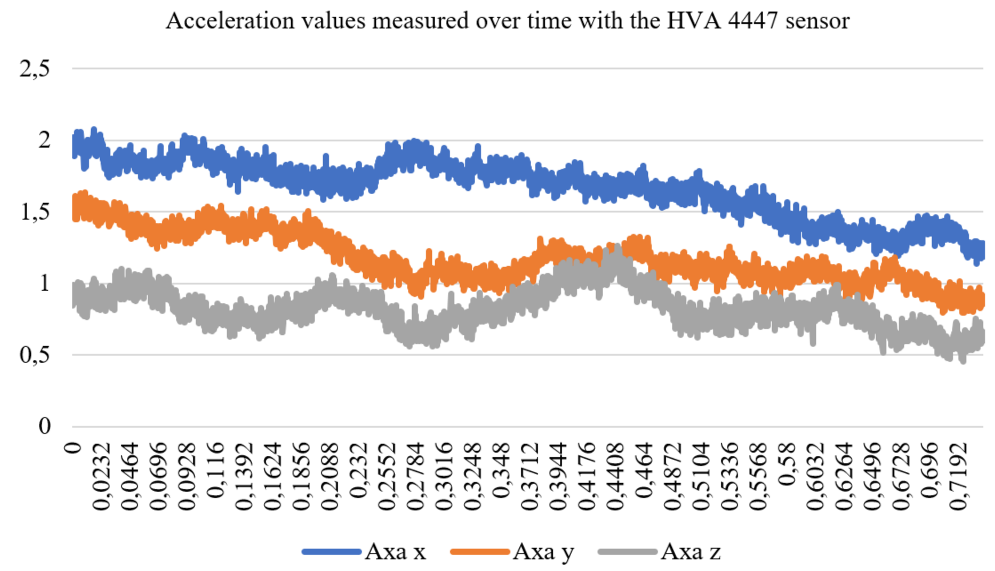


***Fig. 8.*** *Results obtained when measuring acceleration with the HVA 4447 sensor located on the operator's knee*

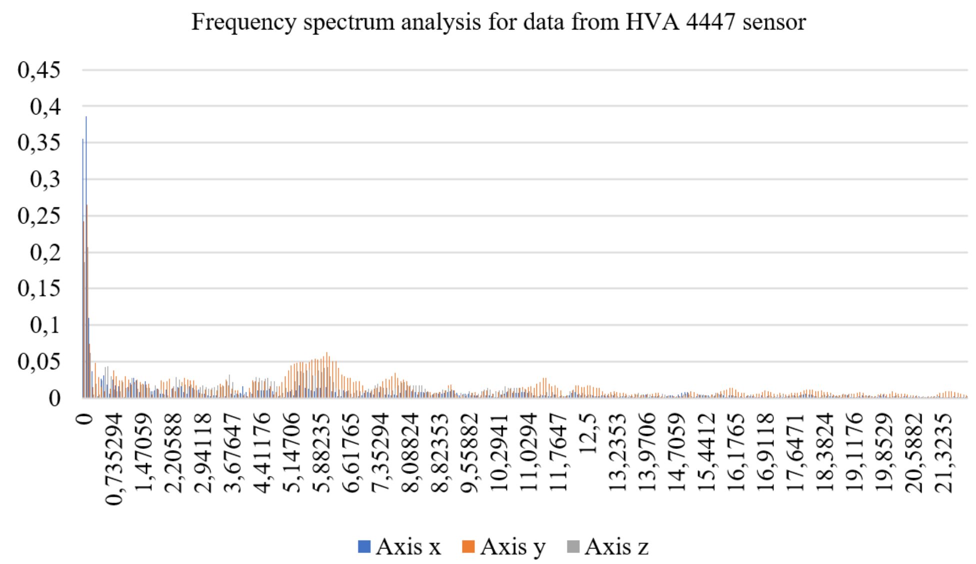


***Fig. 9.*** *Frequency spectrum analysis for data obtained with HVA 4447 sensor*

Considering that a sensor with higher sensitivity (below 10 Hz) was needed, the HVA 4447 accelerometer was used for a new set of measurements. The values obtained for accelerations with this type of sensor and the Fast Fourier transform response to the signal are presented in Tables 4 and 5 and in Figures 8 and 9.

## 4. Validation of the theoretical model

The determinations made with the two types of sensors, on the drill and on the operator, validated the theoretical model to a good extent, the errors being in the range of 2% - 3%.

With the Brüel&Kjaer 4506-B 003 sensor, an average acceleration of 23.61 $m/s^2$ was obtained at idle.

The average acceleration values, measured with the HVA 4447 sensor, were 9.24 $m/s^2$ (idle running); 5.22 $m/s^2$ (in wood); and 5.64 $m/s^2$ (in concrete).

## 5. Conclusions

In several previous studies, the authors attempted to perform the same determinations, but on

N°. 1 - 2025, ISSN 2668-4748; e-ISSN 2668-4756
Article DOI: https://doi.org/10.35219/mms.2025.1.01

the human elbow joint. It was found with certainty that the effect of vibration phenomena on the elbow is more significant than on the knee.

Vibrations generated by rotary hammers can affect knee health, especially for operators who are frequently and long-term exposed to this type of vibration. It is important for both employers and workers to adopt preventive measures to protect joints and reduce the risk of illness.

Reducing the negative effects of vibrations in the knee area can be achieved by using appropriate protective equipment (footwear, knee protectors), regular breaks for workers and proper operator training to use the machine tool efficiently and with minimal health risks.

We believe that in one of the following articles it is imperative to review the most widespread actions taken to combat and prevent the negative effects of vibrations.

## References

**[1]. R. Panaitescu-Liess**, *Biomechanical modeling of the human body under the action of vibrations*, Doctoral thesis, U.T.C.B., Bucharest, 2013.
**[2]. Stănescu (Dogaru) M. G.**, *Biomechanical modeling of human body joints under the action of mechanical vibrations*, Doctoral thesis, U.T.C.B., Bucharest, 2022.
**[3]. Moşneguţu V.**, *Contributions on the dynamics of friction systems with applications in vibration control and damping*, Doctoral thesis, Bucharest, 2008.
**[4]. Moşneguţu V., Chiroiu V.**, *Introduction to mathematical modeling of the knee joint*, Romanian Academy Publishing House, Bucharest, 2013.
**[5]. Cezar Th. Niculescu, *et al.***, *Human Anatomy and Physiology. Compendium*, Corint Educational Publishing house, ISBN 978-606-8609-07-2, 2014.
**[6]. Anne E. Martin, Dario J. Villarreal, Robert D. Gregg**, *Characterizing and modeling the joint-level variability in human walking*, Journal of Biomechanics, 49, p. 3298-3305, 2016.
**[7]. Akio Yamamoto, *et al.***, *Behavioral effect of knee joint motion on body's center of mass during human quiet standing*, Gait & Posture, 41, p. 291-294, 2015.
**[8]. Hyunggwi Song, Heewon Park, Sukyung Park**, *Springy pendulum could describe the swing leg kinetics of human walking*, Journal of Biomechanics, 49, p. 1504-1509, 2016.
**[9]. Raj Desai Anirban, Guha P. Seshu**, *Multibody Biomechanical Modelling of Human Body Response to Direct and Cross Axis Vibration*, Procedia Computer Science, vol. 133, p. 494-501, version of Record 20 July 2018.
**[10]. Chadefaux D., *et al.***, *Development of a two-dimensional dynamic model of the foot-ankle system exposed to vibration*, Journal of Biomechanics, vol. 99, 109547, 23 January 2020.
**[11]. Pavel C., Constantinescu A.**, *Mechanical vibrations*, Matrix Rom Publishing house, Bucharest, ISBN 978-973-755-468-0, 2009.
**[12]. Stefan Seiterle, *et al.***, *Interlimb coordination in body-weight supported locomotion: A pilot study*, Journal of Biomechanics, 48, p. 2837-2843, 2015.
**[13]. *****, https://www.bricodepot.ro/unelte/unelte-electrice/borma-ina-cu-percu-ie-skil-900-w-cu-doua-viteze.html.
**[14]. Fabian van de Bunt, *et al.***, *A novel physiological testing device to study knee biomechanics in vitro*, The Knee, 24, p. 718-725, 2017.
**[15]. Toader D., Dogaru M., Ursache R., Bauşic F.**, *Partial experimental contributions on the validation of biomechanical models of the human body subjected to the action of mechanical vibrations*, Modeling in Civil and Environmental Engineering Magazine, vol. 16, no. 4, p. 25-33, ISSN 2784-1391, 2021.
**[16]. Julia K. Nicholsa, Oliver M. O'Reilly**, *Verifying the equivalence of representations of the knee joint moment vector from a drop vertical jump task*. The Knee, 24, p. 484-490, 2017.
**[17]. Johal P., *et al.***, *Tibio-femoral movement in the living knee. A study of weight bearing and non-weight bearing knee kinematics using 'interventional' MRI*, J Biomech, 38, p. 269-76, 2005.
**[18]. Panaitescu-Liess R., Legendi A., Pavel C.**, *Analysis of a mechanical system's dynamic properties by vibrations measurements*, 34rd National Conference on Mechanics of Solids, Analele Universităţii "Eftimie Murgu", Resiţa, anul XVII, no. 1, ISSN 1453-7397, p. 39-44, Reșița, 16th-18th September 2010.
**[19]. Panaitescu-Liess R., Pavel C.**, *Analysis of dynamic response of the human body as a system with several degrees of freedom from external harmonic perturbations*, RJAV, vol. X, issue 2, ISSN 1584-7284, 2013.
**[20]. *****, *Mechanical Systems and Signal Processing*, vol. 167, Part A, 2021.
**[21]. *****, *Human vibrations*, Brüel & Kjaer Sound and Vibrations Measurement, 2003.
**[22]. *****, *Directive 2002/44/EC of the European Parliament and of the Council of 25 June 2002 on the minimum health and safety requirements regarding the exposure of workers to the risks arising from physical agents (vibration) (sixteenth individual Directive within the meaning of Article 16(1) of Directive 89/391/EEC)*, Official Journal of the European Union 05/Vol.
**[23]. *****, *Decision no. 589 of 12.05.2016 on the minimum requirements for occupational health and safety regarding the exposure of workers to risks generated by mechanical vibrations*, Published: 20.05.2016 in the Official Gazette no. 134-139 art. no. 647 Date of entry into force: 01.01.2017 Pursuant to article 6 of the Law on Occupational Health and Safety no. 18.

THE ANNALS OF “DUNAREA DE JOS” UNIVERSITY OF GALATI
FASCICLE IX. METALLURGY AND MATERIALS SCIENCE
N°. 1 - 2025, ISSN 2668-4748; e-ISSN 2668-4756
Article DOI: https://doi.org/10.35219/mms.2025.1.02

# CHALLENGES REGARDING DIGITALIZATION IN CONSTRUCTION

**Simona STANCA**
Technical University of Cluj-Napoca, Buildings and Management Department, Romania
e-mail: simona.stanca@ccm.utcluj.ro

## ABSTRACT

*In an era marked by rapid change and accelerated technological progress, the construction industry is already experiencing significant transformations due to the implementation of automation and digitalization. Digitalization in construction is an essential process for increasing efficiency, reducing costs, and improving sustainability. However, this transition faces multiple challenges. Among the main obstacles are the resistance to change by traditional firms, the lack of digital skills among employees, and the high costs of implementing advanced technologies. The difficult integration of digital solutions into existing processes, the lack of interoperability between platforms, and cybersecurity concerns are other major barriers. Overcoming these challenges can facilitate a sustainable digital transformation with significant benefits for productivity and building quality. Thus, digitalization becomes not only an opportunity, but also a necessity for the future of the construction industry. The paper analyses how digital technology is revolutionizing the construction sector, highlighting both the advantages and challenges generated by this technological change.*

KEYWORDS: digital technology, construction industry, challenges, digitalization

## 1. Introduction

The construction industry, one of the fundamental sectors of the global economy, is undergoing significant transformation due to digitalization. Digitalization in construction is the process of integrating digital technologies into all stages of a construction project, from planning and design to execution, monitoring, and maintenance.

This involves the use of modern solutions such as building information modelling (BIM) (Fig. 1) [1], Artificial Intelligence (AI), Augmented and Virtual Reality (AR/VR), process automation, and the Internet of Things (IoT).

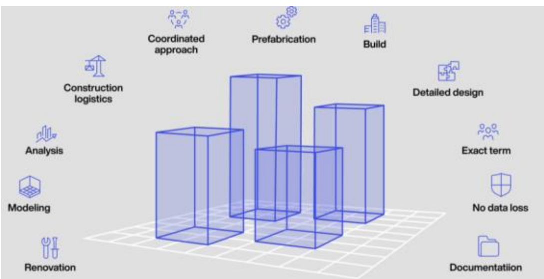


***Fig. 1.** BIM project monitoring strategy* [1]

The adoption of these technologies involves numerous challenges, both technical and organizational.

In a traditional industry, where processes are often slow and manual, the transition to a digital model involves overcoming several obstacles. These challenges are not insurmountable, but they require a strategic approach, investment in training, and the adoption of an open mindset to change in order to fully harness the potential of digitalization in construction [2].

## 2. The importance of using digital technology in construction

The use of digital technology in construction is essential for the modernization and efficiency of the industry, having a significant impact on the way buildings are planned, designed, constructed, and maintained.

The main digital technologies used in construction and their impact on efficiency, sustainability, and safety in the field:

• Computer-Aided Design (CAD) and Building Information Modeling (BIM)

THE ANNALS OF "DUNAREA DE JOS" UNIVERSITY OF GALATI
FASCICLE IX. METALLURGY AND MATERIALS SCIENCE
N°. 1 - 2025, ISSN 2668-4748; e-ISSN 2668-4756
Article DOI: https://doi.org/10.35219/mms.2025.1.02

CAD (Computer-Aided Design) technologies allow the creation of detailed 2D and 3D models of structures, making it easier to view and modify designs before construction. BIM (Building Information Modeling) expands this capability, integrating additional information about materials, costs, and the execution schedule, promoting more efficient collaboration between architects, engineers, and builders [3]. This integration reduces errors and saves time and resources [4].

• Virtual Reality (VR) and Augmented Reality (AR)

These technologies are used for simulations and visualizations of projects before construction begins. Augmented reality can help site staff visualize project information directly in the field, while virtual reality can be used for training and presenting projects to customers (Fig. 2) [5].


***Fig. 2.*** *VR & AR in the Construction Sector* [5]

• Drones and 3D Printing

Drones equipped with cameras and sensors capture aerial images of construction sites, facilitating the monitoring of the progress of the work and periodic inspections. 3D printing technology allows building components to be made quickly and accurately.

This can reduce construction costs and time, and contribute to the creation of innovative structures (Fig. 3) [6].


***Fig. 3.*** *Drone scanning* [6]

• IoT (Internet of Things):

IoT devices are integrated into construction equipment and buildings to collect real-time data, such as the condition of machinery or environmental conditions on the construction site. This data is essential for effective project management.

Due to the complexity that arises in the use of software, hardware, embedded systems, and network ecosystems, it becomes very important to study, understand, and use the appropriate technology for automating a building (Fig. 4) [7].

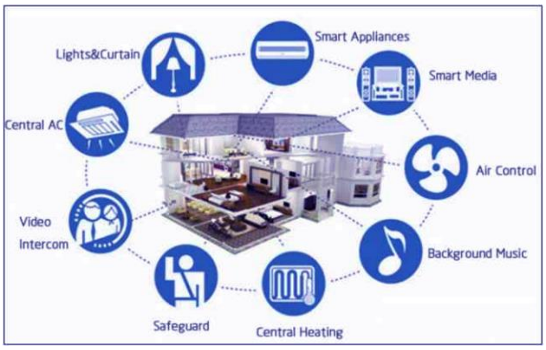


***Fig. 4.*** *Internet of Things applications in buildings* [7]

• Automation and Robotics:

Robots are increasingly being used in construction for tasks such as material handling, welding, or installation, thus reducing working time and exposure to risks for workers [8].

With a fast-paced construction process, the incorporation of robotics technology in construction facilitates construction professionals with quality-assured outcomes and reduced human errors.

• Project Management Software

Digital platforms for project management allow teams to be coordinated, progress to be tracked, resources to be managed, and deadlines to be met, leading to more efficient execution of work [9].

The adoption of these technologies is essential to meet today's challenges and ensure the development of a smarter and more sustainable built environment.

## 3. Advantages and disadvantages of digitalization in construction

Digitalization in construction brings numerous benefits, including increased efficiency, reduced costs, and improved safety, but it also comes with a few challenges [10]. It is essential that these challenges be managed correctly, through investments in training, infrastructure, and security, in order to reap the full benefits of digital technologies in the sector [11].

Nº. 1 - 2025, ISSN 2668-4748; e-ISSN 2668-4756
Article DOI: https://doi.org/10.35219/mms.2025.1.02

Advantages of digitalization in construction:

• Increased efficiency

Digitalization helps to increase efficiency at all stages of the construction process. Digital tools, such as BIM (Building Information Modeling) software, allow the creation of detailed project models, optimizing planning and execution. This reduces working time and reduces the risk of errors.

• Cost reduction

While initial investments in technology can be high, in the long run, digitalization can help reduce costs. Automating processes and monitoring projects more effectively lead to material savings, reduced risks, and better resource management.

• Improving safety

Real-time monitoring technologies, such as drones, can be used to inspect risk areas and ensure safety on the construction site. At the same time, digital models allow the simulation of construction scenarios and the identification of potential problems before the start of work, preventing accidents.

• Improved collaboration

Digital platforms allow for better collaboration between all actors involved in a construction project (architects, engineers, builders, and customers), facilitating the rapid exchange of information and reducing the risk of misunderstandings or miscommunication.

• Sustainability and impact reduction on Environment

Digitalization can contribute to a more efficient management of resources, such as building materials and energy [12, 13]. For example, BIM solutions allow for detailed analysis of a project's energy consumption, identifying solutions to reduce environmental impact.

• Access to advanced data and analytics

Digitalization allows data to be collected and analysed in real time. Thus, project managers can make decisions based on accurate and up-to-date information, which can help to better manage the project and identify possible problems early.

Disadvantages of digitalization in construction:

• High upfront costs

The implementation of digital technologies requires considerable investment in software, equipment and staff training. This can be a barrier for small companies or those that do not have large budgets.

• Resistance to change

In many cases, employees and management teams of construction companies may be reluctant to adopt new technologies, preferring to keep traditional ways of working. This resilience can delay the digitization process and reduce its benefits.

• Lack of qualified personnel

Digital technologies in construction require a specialized workforce, and this requires continuous training. Many workers in the industry lack IT skills, and attracting qualified personnel can be difficult.

• Interoperability issues

The different software solutions used in construction may not be compatible with each other. Lack of standardization can lead to difficulties in integrating data and applications, and this can reduce the overall efficiency of the construction process.

• Cybersecurity

As more data is stored and processed digitally, cybersecurity risks become a major issue. Cyberattacks can compromise sensitive project and client information, and protecting them becomes essential.

• Dependence on technology

Digitalization can create a dependency on technology, and in the event of a technical failure or an interruption of the internet connection, the entire construction process can be blocked. In addition, the existence of errors in the software or incorrect data can lead to serious problems on the construction site.

Digitalization in construction offers multiple benefits, but also significant challenges. To maximize the advantages and minimize the disadvantages, careful planning, investment in training, and the development of an organizational culture open to change are essential.

## 4. Trends for the future of construction from the perspective of digital technology

There are several examples of buildings that use digitized technologies to improve energy efficiency, occupant comfort, and infrastructure management.

• The Edge, Amsterdam, Netherlands

This is one of the smartest office buildings in the world. It uses technologies such as the Internet of Things (IoT), lighting and temperature sensors, and mobile apps that allow employees to adjust their work environment, find available desks, and optimize their routes through the building. The air conditioning and lighting systems are automatically controlled according to the presence and activity of occupants in the rooms (Fig. 5) [14].

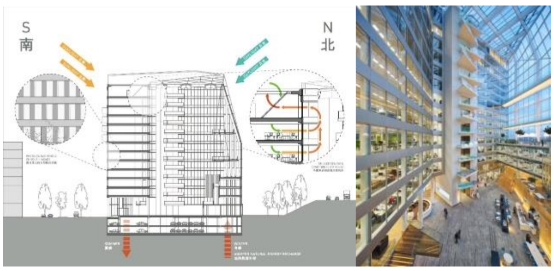


***Fig. 5.*** *The Edge (Amsterdam, Netherlands)* [14]

N°. 1 - 2025, ISSN 2668-4748; e-ISSN 2668-4756
Article DOI: https://doi.org/10.35219/mms.2025.1.02

• Bosco Verticale, Milan, Italy

These buildings are an example of digitized and sustainable urbanism. Although best known for integrating vegetation into the facade, they are equipped with smart technologies that monitor and regulate water and energy consumption, as well as indoor environmental conditions (Fig. 6) [15].


***Fig. 6.*** *Bosco Verticale (Milan, Italia)* [15]

• Marina Bay Sands, Singapore

This complex uses digital technologies to efficiently manage lighting, air conditioning, and access to different areas of the building. In addition, security systems are digitally managed, and the use of sensors to monitor the flow of visitors helps to improve their experience. (Fig. 7) [16, 17].

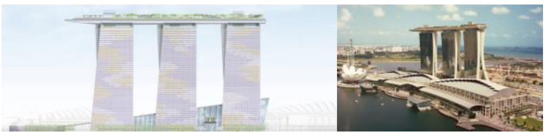

***Fig. 7.*** *Marina Bay Sands (Singapore)* [16, 17]

• The Office, Cluj-Napoca

This office building uses smart technologies for energy management and climate control [18]. The lighting systems are automatically adjusted based on occupancy and available natural light, and the energy consumption is monitored in real time through a BMS system (Fig. 8) [19].

***Fig. 8.*** *The Office, Cluj-Napoca* [19]

These buildings are some examples of how digitized technologies can transform the urban environment to optimize the economic and ecological performance of buildings.

## 6. Conclusions

Digitalization in the construction industry brings multiple benefits, such as streamlining processes, reducing costs, and improving safety on site. However, the deployment of digital technologies faces significant challenges, including resistance to change, high costs, lack of skilled personnel, and interoperability issues between different software solutions [20].

To overcome these obstacles, a well-defined strategy is essential, including:

• Investments in vocational education and training, for the development of employees' digital skills.

• Adoption of standards and regulations that facilitate the integration of new technologies.

• Collaboration between companies, educational institutions, and authorities, to accelerate the digital transition.

• Implementation of cybersecurity measures, to protect data and digital infrastructure.

In conclusion, digitalization is the future of the construction industry, and companies that manage to adopt and integrate new technologies will have a significant competitive advantage.

The transition requires time and resources, but the long-term benefits are considerable, both in terms of operational efficiency and sustainability of construction projects.

## References

**[1].** ***, https://www.team-tda.com/services/bim-management/.

**[2].** ***, https://www.ghid-constructii.ro/despre/digitalizarea-in-mediul-constructiilor-cum-tehnologia-transforma-industria-pas-cu-pas/, accessed in 7.02.2025.

**[3]. Bueno C., Fabricio M. M.**, *Comparative analysis between a complete LCA study and results from a BIM-LCA plug-in*, Autom. Constr., 90, p. 188-200, 2018.

**[4].** ***, https://constructiiedilitare.ro/rolul-tehnologiei-in-constructia-moderna-de-case/, accessed in 7.02.2025.

**[5].** ***, https://www.augray.com/blog/vr-ar-in-the-construction-sector/, accessed in 7.02.2025.

**[6].** ***, https://www.linkedin.com/pulse/transforming-building-documentation-future-drone-scanning-ydlkc., accessed in 8.02.2025.

**[7].** ***, https://data-flair.training/blogs/internet-of-things-applications-in-building/, accessed in 8.02.2025.

**[8].** ***, https://bilboconstruct.ro/utilaje-si-tehnologie-in-constructii/automatizarea-si-robotica-viitorul-constructiilor/, accessed in 8.02.2025.

**[9].** ***, https://www.project-management-romania.ro/articole/transformarea-digitala-in-constructii/, accessed in 8.02.2025.

**[10]. Stanca Simona**, *Improving energy efficiency in a building using passive energy-saving measures*, Journal of Applied Engineering Sciences (JAES), ISSN: 2247-3769 / e-ISSN: 2284-7197, vol. 13(26)2-2023, https://doi.org/10.2478/jaes-2023-0034, 2023.

**[11]. Patranjel Nicoleta**, *Revoluția sustenabilității în construcții: rolul tehnologiilor digitale în respectarea standardelor europene*, URI: http://repository.utm.md/handle/5014/28141, 2024.
**[12]. Gajdzik B., *et al.***, *The influence of the global energy crisis on energy efficiency: A comprehensive analysis*, Energies, 17(4), 947, https://doi.org/10.3390/en17040947, 2024.
**[13]. Stanca Simona**, *Reuse of construction waste*, A 17-a Conferință Internațională Interdisciplinaritatea în Inginerie International Conference Interdisciplinarity in Engineering - INTER-ENG 2023, 5- 6 October 2023, U.M.F.S.T., Târgu Mureș, Procedia Engineering, Parte a seriilor de cărți Lecture Notes in Networks and Systems (LNNS, volumul 926), p. 198-209, ISBN: 978-3-031-54663-1, Online ISBN978-3-031-54664-8, Seria ISSN 2367-3370, DOI. https://doi.org/10.1007/978-3-031-54664-8_19, 2023.
**[14]. *****, https://www.archdaily.com/785967/the-edge-plp-architecture, accessed in 12.02.2025.
**[15]. *****, https://www.archdaily.com/777498/bosco-verticale-stefano-boeri-architetti, accessed in 12.02.2025.
**[16]. *****, https://archello.com/project/marina-bay-sands, accessed in 12.02.2025.
**[17]. *****, https://www.archdaily.com/70186/marina-bay-sands-safdie-architects, accessed in 12.02.2025.
**[18]. Stanca Simona**, *The future of construction from a sustainable materials perspective*, The Annals of "Dunarea de Jos" University of Galati Fascicle IX Metallurgy and Materials Science, ISSN 2668-4748 (Print), 2668-4756 (Online), vol., no. p. 37-42, 2024, DOI: https://doi.org/10.35219/mms.2024.1.05, 2024.
**[10]. *****, https://www.archdaily.com/888983/the-office-cluj-andreescu-and-gaivoronschi, accessed in 12.02.2025.
**[20]. *****, https://www.eubim.eu/wp-content/uploads/2018/02/GROW-2017-01356-00-00-RO-TRA-00.pdf.

THE ANNALS OF "DUNAREA DE JOS" UNIVERSITY OF GALATI
FASCICLE IX. METALLURGY AND MATERIALS SCIENCE
N°. 1 - 2025, ISSN 2668-4748; e-ISSN 2668-4756
Article DOI: https://doi.org/10.35219/mms.2025.1.03

# PACKAGING WASTE MANAGEMENT AND THE MAIN CHALLENGES IN RECYCLING PROCESSES

**Carmelia Mariana BĂLĂNICĂ DRAGOMIR, Geanina Marcela PODARU, Alina Mihaela CEOROMILA, Iulia PĂDURARU GRAUR, Marian Tiberiu COADĂ, Maricica STOICA**
"Dunarea de Jos" University of Galati, Romania
e-mail: Carmelia.Dragomir@ugal.ro

## ABSTRACT

*Separate collection of packaging is an important step towards a circular economy. Setting a mandatory collection rate is an incentive for the development of efficient and well-targeted collection systems at national level, thus increasing the amount of waste sorted and potentially recycled. This article presents a comparative analysis, by waste type, of the evolution of packaging waste recycling, during the period 2008-2022. While in the period 2013-2022 the average recycling rate of packaging waste in EU member states was 65.74%, in Romania the rate was 50.31%, which requires a series of additional efforts. At the national level, during the period 2013-2022, the highest percentage of packaging waste recycling was represented by paper and cardboard (74.35%) and metal (56.02%), with wood waste ranking last, at 23.77%.*

KEYWORDS: packaging waste recycling, circular economy, recycling rate

## 1. Introduction

Since 1950, global production of plastics has increased substantially, driven by their unique properties: high strength-to-weight ratio, high moldability, impermeability to liquids, resistance to physical and chemical degradation, and low cost [1]. As such, they are used in the production of a wide range of products, easily replacing wood, paper, stone, leather, metal, glass, and ceramics. "Plastic" is an umbrella term that encompasses a wide range of materials made from semi-synthetic or synthetic organic compounds [2]. Synthetic polymers are typically prepared by the polymerization of monomers derived from petroleum or gas, and plastics are typically manufactured from these by adding various chemical additives [3].

The dynamic growth of global plastic production in recent decades and the increasing consumption of plastics have led to an increase in the amount of plastic waste generated each year [4]. As a result, the risk of mismanagement of plastic waste and its negative impact on the environment has increased. Mismanagement of waste poses a high risk of leakage and transport to the natural environment and oceans through waterways, winds, and tides [5].

Plastic litter has impacts on both terrestrial and marine environments. Globally, estimates suggest that approximately 80% of ocean plastic comes from land-based sources, with the remaining 20% from marine sources. Marine plastic pollution is caused by fishing fleets that leave behind fishing nets, ropes, and sometimes abandoned ships. For land-based sources, the main contributor is larger plastic litter, including everyday items such as beverage bottles and other types of plastic packaging [6].

New sources of plastic leakage into the environment are also on the rise, posing additional potential threats to both the environment and human health. Microplastics, tiny pieces of plastic less than 5 mm in size, accumulate in the seas, and their small size makes them easy for marine life to ingest [7]. They can also enter the food chain. In total, it is estimated that between 75,000 and 300,000 tonnes of microplastics are released into the environment each year in the EU [8].

As stated in Eurostat - Statistics Explained in 2022, the EU generated an estimated 186.5 kg of packaging waste per inhabitant (varying from 78.8 kg per inhabitant in Bulgaria to 233.8 kg per inhabitant in Ireland). The same source mentions that during the period 2011 to 2022, paper and cardboard were the main packaging waste material in the EU (34.0

N°. 1 - 2025, ISSN 2668-4748; e-ISSN 2668-4756
Article DOI: https://doi.org/10.35219/mms.2025.1.03

million tonnes in 2022), followed by plastic (16.1 million tonnes) and glass packaging waste (15.7 million tonnes) [9].

According to Directive 904/2019, measures must be adopted to significantly reduce the consumption of single-use plastic products by 2026 [10]. Measures may include national consumption reduction targets, measures to ensure that alternatives for the reuse of single-use plastic products are made available at the point of sale to the final consumer, economic instruments to ensure that single-use plastic products are not provided free of charge at the point of sale to the final consumer, and voluntary agreements. EU Member States may impose restrictions on the marketing of packaging that complies with Directive 94/62/EC, in order to prevent waste generation, and to ensure that it is replaced by alternatives that are reusable or do not contain plastic [11].

Packaging must be designed, manufactured, and marketed in such a way that it can be reused or recycled, thereby minimizing its impact on the environment throughout its life cycle and that of the products for which it is intended. Also, taking into account scientific and technological progress, packaging should be designed and manufactured in such a way that chemical substances of concern are reduced to a minimum and replaced as far as possible, in order to ensure a high level of protection for consumers of packaged products and to avoid adverse effects on the environment [12].

Starting in 2025, beverage bottles made of polyethylene terephthalate (PET) will contain at least 25% recycled plastic, and starting in 2030, they will contain at least 30% recycled plastic, calculated as an average for all PET bottles placed on the market in the territory of the member state concerned [13].

## 2. Materials and Methods

After the introduction of stricter legislative requirements through Directive (EU) 2018/852, amending Directive 94/62/EC on packaging and packaging waste (Packaging Waste Directive) the recycling and reuse of packaging waste have become a priority at the EU level. For these reasons, consideration was given to implementing several forms of packing waste recovery, consequently diminishing the final disposal of this type of waste, as well as ensuring permanent monitoring of recycled quantities.

The information used in this article is based on the datasets posted on the website https://ec.europa.eu/eurostat/databrowser/view/env_waspacr/default/table?lang=en regarding packaging waste statistics, for the period 2013 – 2022 [14].

At the national level, the information processed in this article is sourced from information collected annually by the National Institute of Statistics, the data being reported by economic operators according to the reporting obligations established by Ministerial Order 794/2012. The indicator regarding the packaging waste recycling rate by material types in total packaging waste generated (http://statistici.insse.ro:8077/tempo-online/#/pages/tables/insse-table) refers to the packaging waste recycling rate by material types, representing the ratio between the amount of packaging waste recycled (by material type) and the amount of packaging waste generated, expressed as a percentage. The period taken into account is 15 years, from 2008 to 2022 [15].

## 3. Results

In order to reduce the amount of waste deposited in landfills and to reuse significant quantities of materials of different types, but especially with the aim of reducing pollution and environmental impact, all types of packaging materials are constantly being considered, regardless of the base material from which they are made, as well as the processes of recycling all types of packaging at the end of their life cycle (packaging waste), regardless of the area of origin where they were generated (in industry, trade, institutions, the service sector, housing, or any other sources). EU Member States use a range of economic instruments to provide incentives for waste recycling, including incentives through extended producer responsibility schemes and requirements for producers or responsible producer organizations to adopt waste prevention plans.

Despite all these investments, however, in some countries, the recycling rate of packaging waste is quite low. During the period 2013-2022, the average recycling rates of packaging waste in the EU, was 62.69 %. Among the Member States, Slovenia (66.66%), Belgium (81.65%), and the Netherlands (75.19%) had the highest recycling rates of packaging waste. In contrast, the lowest recycling rates of packaging waste were recorded in Malta (37.05%), Hungary (48.42%) and Romania (50.28%).

For the analysed period, the EU-27 average recycling rate of packaging waste varied quite a bit, starting from 65.4% in 2013, with some insignificant increases up to 67.6% in 2017, and then remained relatively stable, the percentage in 2022 being 65.74%.

N°. 1 - 2025, ISSN 2668-4748; e-ISSN 2668-4756
Article DOI: https://doi.org/10.35219/mms.2025.1.03

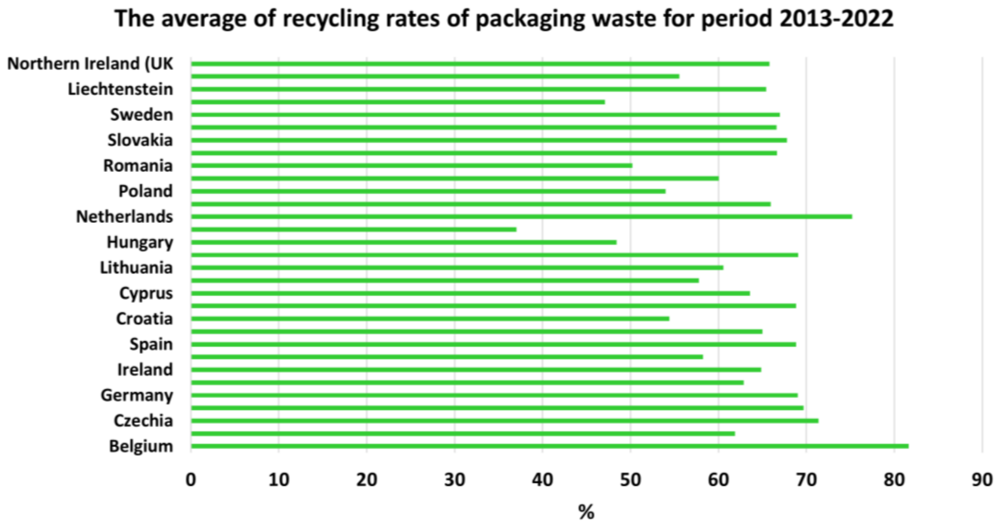


***Fig. 1.*** *The average of recycling rates of packaging waste for period 2013-2022*

In the case of Romania, the average recycling rate of packaging waste was 52.8% in 2013, with an increase of up to 60.4% in 2016-2017, and then followed by a gradual decrease to 38.1% in 2022.

This decrease in the recycling rate is an extremely important aspect that must be addressed by identifying a number of ways to improve the current situation, primarily by educating and raising awareness among the population about the impact of recycling, and investing funds in improving the collection infrastructure.

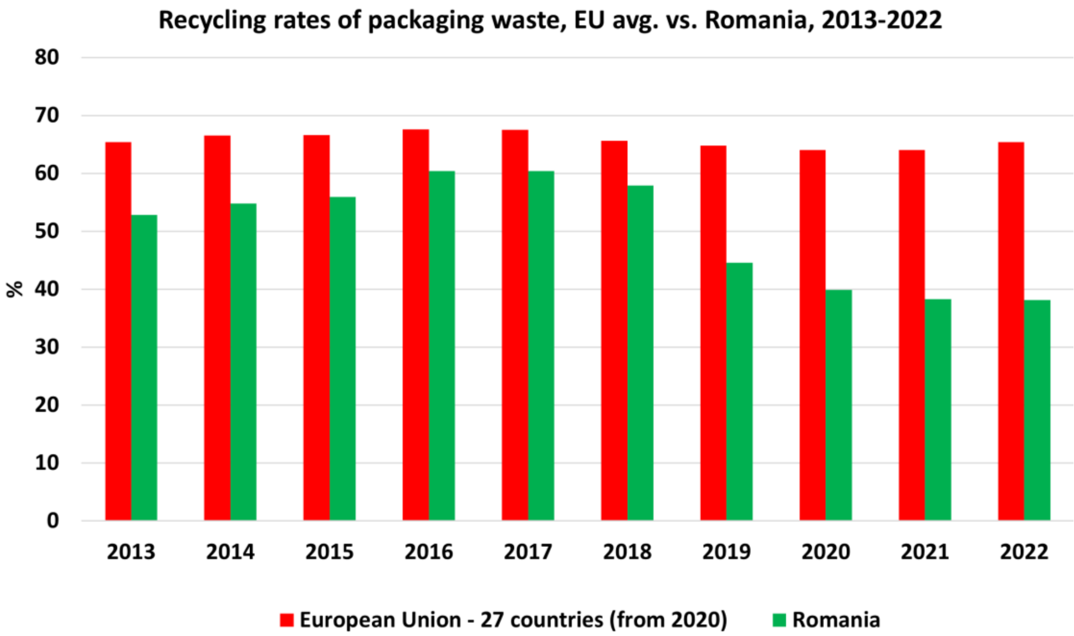


***Fig. 2.*** *Recycling rates of packaging waste, EU avg. vs. Romania, 2013-2022*

As an EU member state, Romania has committed to recycling a certain percentage of packaging waste generated by the population, companies, and institutions. The target set for 2025 is that 65% of total waste will be recycled (plastics 50%; wood 25%; ferrous metals 70%, aluminium 50%, glass 70%, paper and cardboard 75%) and 70% by 2030 (plastics 55%; wood 30%; ferrous metals 80%, aluminium 60%, glass 75%, paper and cardboard 85%).

Since 2005, a series of requirements have been legislated in Romania regarding the management of packaging and packaging waste, and since 2008, the National Institute of Statistics has been collecting

THE ANNALS OF “DUNAREA DE JOS” UNIVERSITY OF GALATI
FASCICLE IX. METALLURGY AND MATERIALS SCIENCE
N°. 1 - 2025, ISSN 2668-4748; e-ISSN 2668-4756
Article DOI: https://doi.org/10.35219/mms.2025.1.03

data on recycled quantities annually. Economic operators, producers, and importers of retail packaging and local public administration authorities are the main parties responsible for reporting the data.

During the period 2008-2022, the highest recycling percentage, 74.35%, is represented by paper and cardboard. In 2008, the recycling rate for paper and cardboard was 61.63% and experienced an upward trend until 2016, when it reached 92.5%, followed by a gradual decrease to 64.13% in 2022.

The average for the 15 years analysed for metal packaging waste was 56.02%, with a series of variations from 50.99% in 2008, reaching the maximum value of 64.18% in 2014, and then decreasing to 42.16% in 2022.

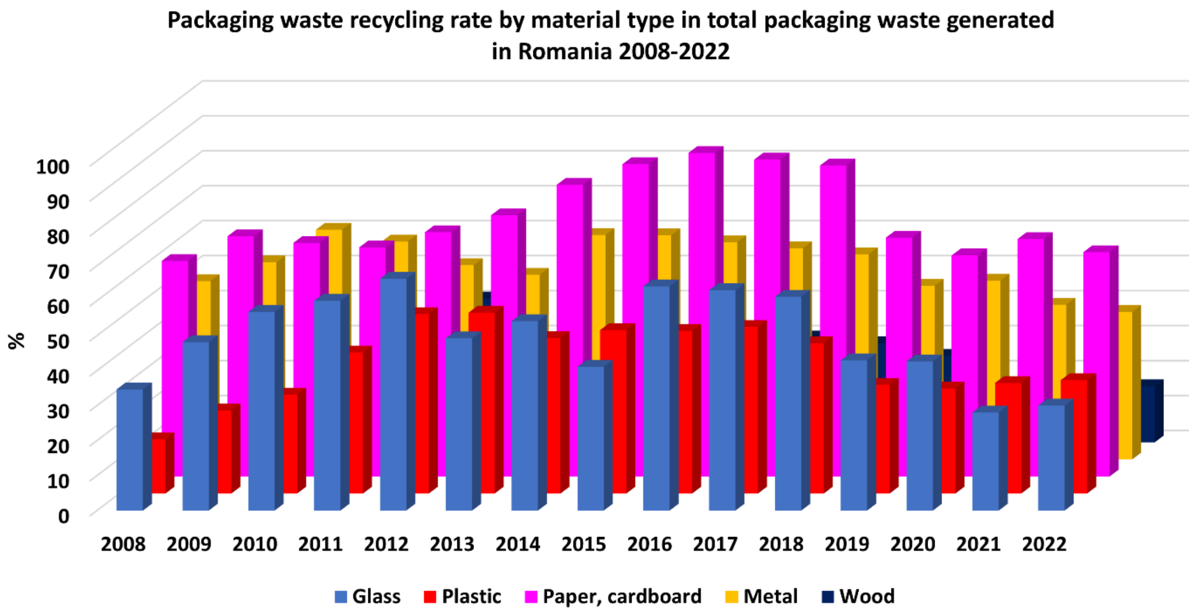


***Fig. 3.*** *Packaging waste recycling rate by material type in total packaging waste generated in Romania 2008-2022*

Glass packaging waste had an average recycling rate of 49.48%, with a series of variations from 34.66% in 2008 to a maximum value of 66.26% in 2012, followed by a decrease and a return to 64.1% in 2016, after which the decreasing trend continued until it reached 30.02% in 2022.

Plastic packaging waste had an average recycling rate of 37.61%, following the same trend as other types of waste, i.e. an upward trend from 2008 (rising from 15.48% to 51.65% in 2013), and then a decrease in this recycling rate to 32.41% in 2022.

The lowest recycling rate is for wooden packaging at 23.77%. In 2008, the recycling rate was 8.26% and reached its peak in 2012 at 41.15%. After a steady decline, the rate reached 15.68% in 2022.

## 4. Conclusions

Turning waste into resources is a key element of the circular economy. Proper implementation of EU waste legislation requires the application of the waste hierarchy, which prioritizes preparing for reuse and recycling, and considers landfilling as the least preferable waste treatment option.

Plastic waste is the subject of EU measures and general waste management targets. To achieve an ambitious and sustainable reduction in global packaging waste generation, targets for the reduction of packaging waste per capita must be set, to be achieved by 2030.

Effective waste management is essential to prevent the negative impacts of waste generation on the environment and health, and to achieve the objectives of the zero-pollution action plan on waste and marine litter. The increased use of packaging, combined with low reuse and recycling rates, hinders the development of a low-$CO_2$ circular economy.

## References

**[1]. Haupt M., Kägi T., Hellweg S.**, *Life cycle inventories of waste management processes*, Data Brief 19, p. 1441-1457, 2018.
**[2]. Gambella C., Maggioni F., Vigo D.**, *A stochastic programming model for a tactical solid waste management problem*, Eur. J. Oper. Res., 273, p. 684-694, 2019.
**[3]. Coelho P., *et al.***, *Sustainability of reusable packaging-current situation and trends*, Resour. Conserv. Recycl., X 100037, 2020.
**[4]. Naayem N.**, *The inherent problem with the global plastic waste trade*, Available online:

https://rethinkplasticalliance.eu/news/the-inherent-problem-with-the- global-plastic-waste-trade, 2021.

**[5]. Eriksen M., *et al.***, *Plastic pollution in the world's oceans: more than 5 trillion plastic pieces weighing over 250,000 tons afloat at sea*, PLoS One, 9 (12), e111913, https://doi.org/10.1371/journal.pone.0111913, 2014.

**[6]. Simões P., Marques R. C.**, *On the economic performance of the waste sector. A literature review*, J. Environ. Manage., 106, p. 40-47, 2012.

**[7]. Alam S. S., Husain Khan A., Khan N. A.**, *Plastic waste management via thermochemical conversion of plastics into fuel: a review*, Energy Sources, Part A Recovery, Util. Environ. Eff., 44 (3), p. 1-20, 2022.

**[8]. Urien B., Kilbourne W.**, *Generativity and self-enhancement values in eco-friendly behavioral intentions and environmentally responsible consumption behavior*, P & M, 28 (1), p. 69-90, 2011.

**[9]. European Commission**, *Database – Eurostat*, https://ec.europa.eu/eurostat/databrowser/view/env_waspacr/default/table?lang=en, 2022.

**[10]. *****, *Directive (EU) 2019/904 of the European Parliament and of the Council of 5 June 2019 on the reduction of the impact of certain plastic products on the environment*.

**[11]. *****, *European Parliament and Council Directive 94/62/EC of 20 December 1994 on packaging and packaging waste*.

**[12]. Herberz T., Barlow C. Y., Finkbeiner M.**, *Sustainability assessment of a single-use plastics ban*, Sustainability, 12 (9), 3746, 2020.

**[13]. *****, *Commission Implementing Decision (EU) 2023/2683 of 30 November 2023 laying down rules for the application of Directive (EU) 2019/904 of the European Parliament and of the Council as regards the calculation, verification and reporting of data on recycled plastic content in single-use plastic beverage bottles*.

**[14]. *****, *Packaging waste statistics, Statistics Explained*, Data extracted on 10 October 2024, https://ec.europa.eu/eurostat/statistics-explained/SEPDF/cache/10547.pdf.

**[15]. *****, *Recycling rate of packaging waste by type of materials in total packaging waste generated*, National Institute of Statistics, http://statistici.insse.ro:8077/tempo-online/#/pages/tables/insse-table, 2022.

THE ANNALS OF “DUNAREA DE JOS” UNIVERSITY OF GALATI
FASCICLE IX. METALLURGY AND MATERIALS SCIENCE
N°. 1 - 2025, ISSN 2668-4748; e-ISSN 2668-4756
Article DOI: https://doi.org/10.35219/mms.2025.1.04

# INTERRELATIONS BETWEEN THE ENTHALPIES OF FORMATION OF THE SULFUR-CONTAINING AMINO ACIDS L-CYSTINE, L-CYSTEINE AND L-METHIONINE

**Stefan Perisanu*[,a], Kathleen F. Edwards[b], Joel F. Liebman[c]**
[a] Department of General Chemistry, Universitatea Națională de Știință și Tehnologie POLITEHNICA, București, Romania
[b] Doctor of Business Administration Program, School of Business, University of Maryland Global Campus, USA
[c] Department of Chemistry and Biochemistry, University of Maryland, Baltimore County, Baltimore, USA
e-mail: stefan.perisanu@upb.ro, kathleen.edwards@faculty.umgc.edu, jliebman@umbc.edu

## ABSTRACT

*L-Cystine, L-cysteine, and L-methionine are among the twenty-two L-α-amino acids from which all proteins are composed. With their unique sulphur atoms, L-cystine, L-cysteine, and L-methionine have been particularly problematic with regard to both qualitative and quantitative understanding of their energetics, most notably their enthalpies of formation. Using thermochemical quantities from calorimetric experiments (enthalpies of combustion, hydrogenolysis, vaporization, and sublimation), high level quantum chemical calculations, and idealized chemical reactions, these enthalpies of formation are derived and interrelated. In a brief epilogue, the conceptual trichotomy of “convenience, anthropocentrism, and folksonomy” is employed to enhance our thermochemical understanding of these species.*

KEYWORDS: L-cystine, L-cysteine and L-methionine; enthalpies of formation, reaction, vaporization and sublimation; disulfides; quantum chemical calculations; sulphur-containing amino acids; trichotomy

## 1. Introduction

Alpha-amino acids and the derived polypeptides and proteins are essential for living organisms, e.g., all enzymes, structural biomaterials (e.g., collagen, elastin, keratin), general health (glutathione, HDL vs. LDL cholesterol, insulin, thyroxine), oxygen and electron metabolism (haemoglobin, the diverse cytochromes), and vitamins (folic acid). Accordingly, knowledge of their energetics is an indispensable part of the fundamental understanding of life. In turn, to understand proteins implies it is desirable to know the energetics of their component α-amino acids. The values of their enthalpies of formation are an essential part of this knowledge. One of the current authors (SP) recently reviewed this topic [1], wherein results from experimental calorimetric measurements and both quantum chemical and group additivity calculations were presented.

Particularly interesting and problematic amino acids include the disulfide L-cystine, along with its reduced (thiol) counterpart, L-cysteine, for which the reported enthalpy of formation values in the solid state are numerous and disparate, and the gas phase data are problematic. We opt to discuss only the values suggested in [2], because they explicitly interweave contemporary experimental practice and high-level theory.

## 2. Discussion

Unlike most other studies of the energetics of amino acids [1], and likewise of many other highly functionalized organic compounds, calorimetric and computational results here are simultaneously given for both the condensed phase (solid) and gas phase species. L-cystine and L-cysteine are abbreviated in this paper as Cys-S-S-Cys and Cys-SH, respectively, to emphasize the sulphur atoms, as opposed to CYT and CYS, without any stereochemistry expressed from [2], their enthalpies of formation are:

$$\Delta_f H_m^o \text{ (Cys-S-S-Cys, s)} = -1045 \pm 2 \text{ kJ mol}^{-1}$$
$$\Delta_f H_m \text{ (Cys-S-S-Cys, g)} = -761 \pm 10 \text{ kJ mol}^{-1}$$

THE ANNALS OF "DUNAREA DE JOS" UNIVERSITY OF GALATI
FASCICLE IX. METALLURGY AND MATERIALS SCIENCE
N°. 1 - 2025, ISSN 2668-4748; e-ISSN 2668-4756
Article DOI: https://doi.org/10.35219/mms.2025.1.04

$\Delta_f H_m^o$ (Cys-SH, s) = -529 ± 1 kJ mol$^{-1}$
$\Delta_f H_m$ (Cys-SH, g) = -383 ± 2 kJ mol$^{-1}$

All of these quantities, except that of gaseous L-cystine, are from direct experimental measurements. The value $\Delta_f H_m^o$ (Cys-S-S-Cys, g) = -761 kJ·mol$^{-1}$ was obtained using Gaussian-3 theory, at the G3(MP2)//B3LYP and/or G3 levels.

In the current paper, we will revisit the enthalpies of formation of L-cystine and L-cysteine, and thereby also that of the remaining sulphur-containing amino acid, L-methionine.

For our first approach, we will consider not only the enthalpies of formation of either L-cystine or L-cysteine per se, but rather the biochemically relevant hydrogenolysis/redox reaction that interrelates them. This hydrogenolysis redox reaction is most simply written as:

$$\text{Cys-S-S-Cys} + H_2 \rightarrow 2\ \text{Cys-SH} \quad (1)$$

From the above experimental values for the solid phase species [2], the enthalpy for this reaction is -13 ± 3 kJ mol$^{-1}$. We start our analysis by discussing the energetics of the hydrogenolysis reactions of general disulfides as found in the gas phase.

$$\text{RS-SR} + H_2 \rightarrow 2\text{RSH} \quad (2)$$

We consider the hydrocarbon-based R groups: $CH_3^-$, $C_2H_5^-$, $(CH_3)_2CH^-$, $(CH_3)_3C^-$, and $C_6H_5^-$. All the relevant thermochemical data in Table 1 are taken from the monograph of Pedley [3].

***Table 1.*** *Enthalpy of gas phase reaction (2) with attached groups R (in kJ mol$^{-1}$)*

| R | $\Delta_f H_m$ (RSH, g) | $\Delta_f H_m$ (RS-SR, g) | $\Delta H_{rkn2}$ |
|---|---|---|---|
| $CH_3^-$ | -23 ± 1 | -25 ± 1 | -21 ± 2 |
| $C_2H_5^-$ | -46 ± 1 | -75 ± 1 | -17 ± 2 |
| $(CH_3)_2CH^-$ | -76 ± 1 | | |
| $(CH_3)_3C^-$ | -110 ± 1 | -201 ± 2 | -19 ± 2 |
| $C_6H_5^-$ | 111 ± 1 | 244 ± 4 | -22 ± 4 |

Group additivity calculations (throughout this paper, taking input values from [4]) result in an estimated value of -18 kJ mol$^{-1}$ for reaction (2) when the sulphur atoms are bound to a sp$^3$ carbon atom. Almost the same value (-19 kJ mol$^{-1}$) is predicted when a benzenoid carbon is involved, although group contributions differ considerably. From our newly derived disulfide and thiol enthalpy of formation interrelation, the enthalpy of formation of gaseous L-cystine equals -746 ± 5 kJ mol$^{-1}$. Equivalently, within the associated uncertainties, the enthalpies of formation and reaction, for cysteine and cystine are consistent with those of other pairs of thiols and disulfides. These highly functionalized amino acids of interest are "normal", despite the presence of numerous functional groups and numerous conformers in both species.

Let us now ask about the energetics of the earlier reaction (2) as applied to condensed phase species. The results are shown in Table 2.

***Table 2.*** *$\Delta_f H_m^o$ (lq) of alkyl participants in reaction (2) as found in related thiols and disulfides and the derived reaction enthalpy $\Delta H_{rkn2}$ (in kJ mol$^{-1}$)*

| R | $\Delta_f H_m^o$ (RSH, lq) | $\Delta_f H_m^o$ (RS- SR, lq) | $\Delta H_{rkn2}$ |
|---|---|---|---|
| $CH_3^-$ | -47 ± 1 | -63 ± 1 | -31 ± 2 |
| $C_2H_5^-$ | -74 ± 1 | -120 ± 1 | -28 ± 2 |
| $(CH_3)_2CH^-$ | -106 ± 1 | | |
| $CH_3CH_2CH_2^-$ | -100 ± 1 | -172 ± 1 | -28 ± 2 |
| $(CH_3)_3C^-$ | -141 ± 1 | -255 ± 2 | -27 ± 2 |
| $CH_3(CH_2)_3^-$ | -125 ±1 | -223 ± 2 | -27 ± 2 |
| $(CH_3)_2CHCH_2^-$ | -132 ± 1 | -233 ± 1 | -33 ± 2 |

It is seen that this liquid-phase reaction has the nearly constant enthalpy of -29 ± 3 kJ mol$^{-1}$, compared to -13 ± 3 kJ mol$^{-1}$ for the solid-phase cystine-cysteine.

What, then, about the thermochemistry of the solids? We may ask about "special" interactions found in L-cystine compared to that of other amino acids. Most amino acids have one positive nitrogenous group and one negative carboxylate group. Accordingly, in the condensed phase of amino acids, there are strong electrostatic interactions, as documented by the lack of volatility of these species.

N°. 1 - 2025, ISSN 2668-4748; e-ISSN 2668-4756
Article DOI: https://doi.org/10.35219/mms.2025.1.04

L-cystine, an amino acid with two positive nitrogenous groups and two negative carboxylate groups, is plausibly anticipated to be involatile and, given its composition and structure, it is also likely to be thermally labile. Indeed, its fusion process at 260.5 °C (the melting point) has been shown to be irreversible [5].

How does the "special" charge distribution in L-cystine affect the enthalpy of formation for the solid species? Is the enthalpy of sublimation enhanced because it has more charges than the other amino acids, in particular L-cysteine? Or has the enthalpy of sublimation reduced because the large dipole moment of L-cysteine has plausibly been effectively replaced by a quadrupole composed of the two positive and two negative charges arising from the two "fragments"? Or is the enthalpy of sublimation a meaningless quantity because the compound decomposes upon melting, and a fortiori boiling, so it corresponds to an irreversible process? There is yet another answer: in cystine, there is no electrostatic effect of the charges of one cysteine on the other, such that all intermolecular electrostatic interactions are the sum of the two cysteine fragments. Indeed, since the -S-S- dihedral angle is approximately 90o, all quadrupole interactions deriving from the two ($NH_3^+$ ••• $COO^-$) dipoles essentially vanish, and the electrostatic contribution to the interaction of L-cystine with other molecules as manifested by the sublimation enthalpy, is twice that of two L-cysteines.

A quick investigation of the literature [3] shows, from a thermochemical perspective, that cystine and diphenyl disulfide are alone among the disulfides, and cysteine for the thiols, that are solids at STP. It is to be noted that the enthalpy of sublimation of L-cystine has been suggested to be almost the same as twice the enthalpy of sublimation of L-cysteine [2]. Relatedly, from a surprisingly simple and successful estimation approach for enthalpies of vaporization [6, 7], the desired quantity for a general disulfide, RS-SR, is very nearly twice that of the corresponding thiol, RSH. That this relation also holds for R = $-CH_2CH(NH_3^+)COO^-$ in the solid phase (and R = $-CH_2CH(NH_2)COOH$ in the vapor phase) suggests there is little interaction between these groups within a given cystine molecule, regardless of the phase. (We now acknowledge that in the current paper we are assuming the additivity of substituent effects on phase-change enthalpies. This is equivalent to ignoring any effects from interactions between functional groups on a given molecule in the solid phase- in contradiction to what is done in the considerably less simple, but numerically more successful, estimation approach of Chickos *et al.* [8]).

An alternative approach to the enthalpy of formation of gaseous L-cystine relates to the enthalpy of formation of L-methionine, (L-Met), in which R = $-(CH_2)_2SCH_3$. The enthalpy of formation of L-methionine reported by Roux *et al.* [9] is used in this study, together with the following relation (3), assumed valid for sulphides with innocuous groups chosen for R:

$$\Delta_f H_m(\text{L-Met, g}) - ½\Delta_f H_m(\text{Cys-S-S-Cys, g}) = \Delta_f H_m^o(CH_3SCH_2CH_2R\text{, g}) - ½[\Delta_f H_m^o(RCH_2S\text{-}SCH_2R\text{, g})] \quad (3)$$

Wherein we now introduce the definition:

$$\delta_4(R) = \Delta_f H_m(CH_3SCH_2CH_2R\text{, g}) - ½[\Delta_f H_m(RCH_2S\text{-}SCH_2R\text{, g})] \quad (4)$$

We now ask: How constant is this difference quantity $\delta_4(R)$? The admittedly sparse available data for the general sulfides and disulfides are given in Table 3.

***Table 3**. $\Delta_f H_m^o$ (g) of participants in reaction (4) and the derived enthalpy difference $\delta_{6(}R)$ (in kJ mol$^{-1}$)*

| R | $\Delta_f H_m$ ($CH_3SCH_2CH_2R$, g) | ½{$\Delta_f H_m$ ($RCH_2S$-$SCH_2R$), g)} | $\delta_4$(R) |
|---|---|---|---|
| $CH_3^-$ | -82 ± 1 | -37 ± 1 | -45 ± 2 |
| $C_2H_5^-$ | -102 ± 1 | -59 ± 1 | -43 ± 2 |
| $(CH_3)_2CH^-$ | -122 ± 2 | -80 ± 2 | -42 ± 3 |

We find the near constancy of $\delta_4$(R) as -43 ± 3 kJ mol$^{-1}$); thus, we hereby deduce that the difference between gas phase enthalpies of formation of L-methionine and ½(L-cystine), i.e., $\Delta_f H_m$(L-Met, g) – ½$\Delta_f H_m$(Cys-S-S-Cys, g), equals -43 ± 3 kJ mol$^{-1}$. Earlier we asserted $\Delta_f H_m$(Cys-S-S-Cys, g) = -761 ± 10 kJ·mol$^{-1}$ and one half of this value is –380 kJ·mol$^{-1}$. Disparate values for the enthalpy of formation of gaseous L-methionine, $\Delta_f H_m$(L-Met, g), ranging from -413 to -442 kJ mol$^{-1}$, are suggested in References [1, 9-13]. We find here that the value found calculated as -380 + (-43) = -423 kJ mol$^{-1}$ is in complete agreement with the value -420 ± 10 kJ mol$^{-1}$ recommended by Roux *et al.* [9].

N°. 1 - 2025, ISSN 2668-4748; e-ISSN 2668-4756
Article DOI: https://doi.org/10.35219/mms.2025.1.04

We close with a preliminary discussion of yet another thermochemical comparison. We note that, with the exception of the cyclic L-proline, all α-amino acids found in proteins may be alternatively written as either $R\text{-}CH(NH_3^+)COO^-$ (for solids) or $R\text{-}CH(NH_2)COOH$ (for gases). For LL-cystine we have ½ [$-CH_2SSCH_2^-$], for L-cysteine, R = $HSCH_2^-$, and methionine, R = $CH_3SCH_2CH_2^-$. Earlier in this paper, we asked how “innocuous” the various hydrocarbon-based groups are, such as methyl, ethyl and phenyl. We now briefly ask the related question: how innocuous are $-CH(NH_3^+)COO^-$ (for solids) and $-CH(NH_2)COOH$ (for gases)? For the current study, we will now consider only gaseous species and discuss only $-CH(NH_2)COOH$, where we use the earlier suggested enthalpies of formation for the amino acid. We ask whether $-CH(NH_2)COOH$ is “replaceable” by the isoelectronic $-CH(CH_3)C(=CH_2)CH_3$ and/or the roughly isosteric $-CH(CH_3)CH(CH_3)_2$. There being almost no thermochemical information on compounds with these latter groups, we now ask about the simpler hydrocarbon group isopropyl $-CH(CH_3)_2$ containing species. Let us accordingly introduce the definition:

$$\delta_5(R) = \Delta_f H_m([R\text{-}CH(NH_2)COOH, g) - \Delta_f H_m(R\text{-}CH(CH_3)_2, g) \tag{5}$$

and present the derived $\delta_5(R)$ values in Table 4.

***Table 4.*** *The gas phase enthalpies of formation for the sulphur-containing amino acids, their corresponding simple hydrocarbon analogues, and the derived enthalpy difference (in kJ mol⁻¹)*

| R- | $\Delta_f H_m$(R-CH(NH₂)COOH, g) | $\Delta_f H_m$(R-CH(CH₃)₂, g) | $\delta_5$(R) |
|---|---|---|---|
| ½[$-CH_2SSCH_2^-$] | -380 ± 7 | -88 ± 1 | -292 ± 7 |
| $HSCH_2^-$ | -383 ± 2 | -87 ± 1 | -296 ± 2 |
| $CH_3SCH_2CH_2^-$ | -420 ± 10 | -129 ± 3 [a] | -291 ± 10 |

[a] This value was obtained by asserting near thermoneutrality (as from group additivity reasoning) for the gas phase reaction (6) wherein $R^1 = CH_3SCH_2CH_2^-$ and $R^2 = CH_3^-$

$$R^1S\text{-}SR^1 + R^2S\text{-}SR^2 \rightarrow 2R^1S\text{-}SR^2 \tag{6}$$

A consensus value of -293 ± 5 kJ mol⁻¹ may thus be suggested for the difference of the enthalpy of formation between a gaseous amino acid and its isopropyl hydrocarbon counterpart. Indeed, a consistent difference value is found for the simplest example, glycine and propane, wherein R = H, with enthalpies of formation of -394 ± 2 from [14-18] and -105 ± 1 from [3], respectively. The resulting difference is -289 ± 2 kJ mol⁻¹.

Given that the amino acids of interest are “normally” found in their solid phase, the reader may naturally ask about the corresponding difference quantity of Eq. 5 for solids. We are unfortunately thwarted here by the absence of the desired enthalpy of formation data for the isopropyl species in their solid phase.

## 3. Conclusions

We now acknowledge other, likewise high level, quantum chemical calculations [14, 15, 18] from which the enthalpy of formation of L-cysteine, but generally not of L-cystine, may be found. The values selected by us for the enthalpies of formation of the three sulphur-containing amino acids L-cystine, L-cysteine, and L-methionine follow the thermochemical interrelations found for simpler (i.e., less functionalized) organic sulphur compounds containing the same -SH and -S-S-bonds. The interrelations introduced in this article were explained by structural effects and are compatible with findings from diverse calorimetric experiments, quantum chemical calculations, as well as group additivity estimations of both enthalpies of formation and phase transition enthalpies.

It is to be noted that L-cystine is composed of two chiral L-cysteine moieties, and so L-cystine should have been named LL-cystine. There is the enantiomer, accordingly named DD-cystine, which has identical physical and chemical, but not biological, properties to the natural LL-species. However, there is also an additional diastereomer in which the chirality of the two “component” amino acids is opposite. Indeed, there is such a species, historically called “meso-cystine” (and abbreviated as m-CYT) that has been generally ignored [19-21]. How stable is it? There are no calorimetric investigations for this latter species. However, L-cystine, i.e., the above LL species, has been shown to slowly racemize in aqueous solutions of strong acids to a mixture of the above diastereomers [19, 21]. The comparable abundance of these chiral and meso-species [19] suggests they have nearly identical Gibbs free energies, and very plausibly also nearly identical enthalpies. In other words, LL-cystine is expected to thermochemically behave like the simpler achiral disulfides that we also discuss in our analysis in this article.

## 4. Epilogue

We conclude our study with an epilogue devoted to trichotomies, the division of an attribute, concept, or class of objects or phenomena into three parts or categories, much as a dichotomy is the much more common word for division into two parts or categories. Some examples of trichotomies that are relevant to our study come to mind. The first relates to macromolecules of biochemical significance. We recognize proteins (polypeptides), polysaccharides (e.g., cellulose), and nucleic acids (both DNA and RNA in their multiple forms) as three such examples. Our concern in the current study is only with proteins, and indeed, such species considered alone, and thereby we ignore other classes of biomolecules such as histones, glycoproteins, and peptide nucleic acids.

The three major categories of biochemically significant dicoordinated, divalent sulphur-containing compounds are disulfides (e.g., L-cystine), thiols/mercaptans (e.g., L-cysteine), and sulphides/thioethers (e.g., L-methionine). We hereby acknowledge, and then choose to ignore, species such as the trisulfide (-S-S-S-) analogue of L-cystine, the hydropersulfide (-S-SH) analogue of L-cysteine, and the ethyl (-S-$C_2H_5$) analogue of methionine (quite sensibly called "ethionine"). After all, they lack the desired thermochemical data for us to proceed.

Chemical reactions may be exothermic, plausibly (or nearly) thermoneutral, or endothermic. The reaction of L-cystine and $H_2$ resulting in L-cysteine is exothermic for the two solid amino acids and plausibly thermoneutral for the gaseous species. Racemization of L-cysteine to form D-cysteine is thermoneutral. The homolytic S-S cleavage reaction of L-cystine to form a pair of L-cysteinyl radicals is endothermic.

It is unambiguous that many α-amino acids are convenient to study - how else do we understand that there are at least 15 calorimetric studies on glycine [1, 22] (the earliest dates to 1884)? For reasons cited in the Introduction, we recall the importance of these species for the functioning of living organisms, most assuredly for us as human beings, and so we may say their study is people-centered and anthropocentric. We also emphasize that α-amino acids have several subclasses such as "acidic" and "dicarboxylic acid" (cf. aspartic and glutamic acid), "basic" and diamines (cf. arginine, lysine, histidine), and the aforementioned "sulphur-containing" species. We hereby recall the conceptual utility and power of understanding general chemical phenomena in terms of the trichotomy: "convenience, anthropocentrism and folksonomy" [23, 24].

## References

**[1]. Perişanu St., Gheorghe D., Neacsu A.**, *The enthalpy of formation of l-α-amino acids*, Insights in Chemistry and Biochemistry, 1, ICBC MS.ID.000515, DOI: 10.33552/ICBC.2021.01.000515, 2020.

**[2]. Roux M. V., *et al.***, *Experimental and computational thermochemical study of sulfur-containing amino acids: L-cysteine, L-cystine, and L-cysteine-derived radicals. S-S, S-H, and C-S bond dissociation enthalpies*, J. Phys. Chem. B, 114, p. 10530-10540, DOI: 10.1021/jp1025637, 2010.

**[3]. Pedley J. B.**, *Thermochemical data and structures of organic compounds*, TRC data series, vol. 1, TRC, College Station, 1994.

**[4]. Domalski E. S., Hearing E. D.**, *Estimation of the thermodynamic properties of C–H–N–O–S–Halogen compounds at 298.15 K*, J. Phys. Chem. Ref. Data, 22, p. 805-1159, DOI: 10.1063/1.555927, 1993.

**[5]. Foces-Foces C., Roux M. V., Notario R., Segura M.**, *Thermal behavior and polymorphism in medium-high temperature range of the sulfur containing amino acids L-cysteine and L-cystine*, J. Therm. Anal. Calorim, 105, p. 747-756, DOI: 10.1007/s10973-011-1302-6, 2011.

**[6]. Acree W. Jr., Chickos J. S.**, *Phase Transition Enthalpy Measurements of Organic and Organometallic Compounds. Sublimation, Vaporization and Fusion Enthalpies From 1880 to 2015*, Part 1. C1 - C10. J. Phys. Chem. Ref. Data, 45, 033101/1-033101/565, DOI: 10.1063/1.4948363, 2016.

**[7]. Acree W. Jr., Chickos J. S.**, *Phase Transition Enthalpy Measurements of Organic and Organometallic Compounds and Ionic Liquids. Sublimation, Vaporization, and Fusion Enthalpies from 1880 to 2015*, Part 2, C11-C192, J. Phys. Chem. Ref. Data, 46, 013104/1-013104/532, DOI: 10.1063/1.4970519, 2017.

**[8]. Chickos J. S., Hesse D. G., Liebman J. F., Panshin S. Y.**, *Estimations of the heats of vaporization of simple hydrocarbon derivatives at 298 K*, J. Org. Chem., 53, 3424, DOI: 10.1021/jo00250a004, 1988.

**[9]. Roux M. V., *et al.***, *The enthalpy of formation of methionine revisited*, J. Phys. Org. Chem., 25, p. 916-924, DOI: 10.1002/poc.2961, 2012.

**[10]. Chickos J. S., Hesse D. G., Liebman J. F.**, *Estimating vaporization enthalpies of organic compounds with single and multiple substitution*, J. Org. Chem., 54, p. 5250-5256, DOI: 10.1021/jo00283a016, 1989.

**[11]. Sabbah C. Mindakis**, *Thermodynamique de substances soufrees. II. Etude thermochimique de la l-cysteine et de la l-methionine*, Thermochim. Acta, 43, p. 269-277, DOI: 10.1016/0040-6031(81)85184-2, 1981.

**[12]. Yang X. W., *et al.***, *Determination of combustion energies of thirteen amino acids*, Thermochim. Acta, 329, p. 109-115, DOI: 10.1016/S0040-6031(99)00002-7, 1999.

**[13]. Notario R., *et al.***, *Experimental and computational study on the energetics of N-acetyl-L-cysteine*, J. Chem. Thermodynam., 73, p. 57-61, DOI: 10.1016/j.jct.2013.08.026, 2014.

**[14]. Dorofeeva O. V., Ryzhova O. N.**, *Gas-Phase Enthalpies of Formation and Enthalpies of Sublimation of Amino Acids Based on Isodesmic Reaction Calculations*, J. Phys. Chem. A, 118, p. 3490-3502, DOI: 10.1021/jp501357y, 2014.

**[15]. Karton A., *et al.***, *Heats of formation of the amino acids re-examined by means of W1-F12 and W2-F12 theories*, Theor Chem Acc, 133, p. 1-15, DOI :10.1007/s00214-014-1483-8, 2014.

**[16]. Dorofeeva O. V., Ryzhova O. N.**, *Revision of standard molar enthalpies of formation of glycine and L-alanine in the* *gaseous phase on the basis of theoretical calculations*, J. Chem. Thermodyn, 41, p. 433-438, DOI: 10.1016/j.jct.2008.12.001, 2009.

**[17]. Stover L., *et al.***, *Fundamental Thermochemical Properties of Amino Acids: Gas-Phase and Aqueous Acidities and Gas-Phase Heats of Formation*, J. Phys. Chem. B, 116, p. 2905-2916, DOI: 10.1021/jp207271p, 2012.

**[18]. Ruscic B., Bros D. H.**, *Accurate and reliable thermochemistry by data analysis of complex thermochemical networks using Active Thermochemical Tables: the case of glycine thermochemistry*, Faraday Discuss, 256, p. 345-372, DOI: 10.1039/D4FD00110A, 2025.

**[19]. Loring H. S., du Vigneaud V.**, *The isolation and characterization of mesocystine*, J. Biol. Chem., 102, p. 287-295, 1933.

**[20]. Apostolos A. J., *et al.***, *Facile Synthesis and Metabolic Incorporation of m-DAP Bioisosteres Into Cell Walls of Live Bacteria*, ACS Chem. Biol., 15, p. 2066-2075, DOI: 10.1021/acschembio.0c00618, 2020.

**[21]. Jacobson S. J., Wilson C. G., Rapoport H.**, *Mechanism of cystine racemization in strong acid*, J. Org. Chem., 28, p. 1074-1077, DOI: 10.1021/jo00922a013, 1974.

**[22]. Domalski E. S.**, *Selected values of heats of combustion and heats of formation of organic compounds containing the elements carbon, hydrogen, nitrogen, oxygen, phosphorus, and sulfur*, J. Phys. Chem, p. 221-277, DOI: 10.1063/1.3253099, Ref. Data, 1972.

**[23]. Edwards K. F., Liebman J. F.**, *Amphoteric, Amphihydric and Ambisaline: Are These Descriptive Concepts Manifestations of Convenience, Anthropocentrism, or Folksonomy?*, Intl. J. Chem. Model., 3, p. 213-226, 2011.

**[24]. Edwards K. F., Perişanu St., Liebman J. F.**, *The Aromaticity of Benzene and the Lack of Aromaticity of Cyclooctatetraene: Is Our Calorimetric Perspective a Manifestation of Convenience, Anthropocentrism, or Folksonomy*, Intl. J. Chem. Model, 5, p. 51-65, 2013.

THE ANNALS OF "DUNAREA DE JOS" UNIVERSITY OF GALATI
FASCICLE IX. METALLURGY AND MATERIALS SCIENCE
N°. 1 - 2025, ISSN 2668-4748; e-ISSN 2668-4756
Article DOI: https://doi.org/10.35219/mms.2025.1.05

# AUTOMATED PROCESSING OF MECHANICAL TEST DATA FOR VARIOUS COMPOSITE MATERIALS USING MATLAB

**Vasile BRIA, Marius BODOR***
"Dunarea de Jos" University of Galati, Romania
e-mail: marius.bodor@ugal.ro

## ABSTRACT

*The behaviour of composite materials during the mechanical testing process might exhibit, in some situations, very different patterns compared to those of conventional materials. This is why the eventual automation of data processing might require additional steps towards obtaining realistic results from mechanical testing. The present work addresses this issue by proposing an algorithm written using MATLAB software and applying it in processing data from mechanical testing of selected composite materials with various compositions and behaviours.*

KEYWORDS: MATLAB; data collection; mechanical characterizations

## 1. Introduction

The new materials industry, like many other fields, is constantly changing, and this leads to the design of new materials with enhanced mechanical properties. The most relevant examples are composite materials, regardless of their type. By definition, a composite material is an assembly consisting of at least two components of different natures and behaviours, provided that they do not interact chemically, so that the material formed has superior characteristics [1].

Recently, such materials have been used in almost all fields, from medicine, sports, to the aerospace field. The use of a composite material requires detailed knowledge of the mechanical behavior.

The mechanical characterization of a material can be done according to a set of standard tests. For the characterization of a material, two types of tests are performed: static and dynamic. Dynamic tests are aimed at describing fatigue behaviour, and static tests are aimed at describing the mechanical behaviour of materials under tension, compression and bending [2].

The branch of science that deals with the characterization of materials, of any kind, is mechanics of materials. For each of the three static tests, the description of a material requires the analysis of the stress/strain characteristic curve, and following the analysis of the characteristic curve, different parameters can be calculated that describe the behaviour of the tested material [3].

In general, test equipment only measures force and displacement, and machine software can generate both graphs and specific parameter values [2]. Information technology plays an important role in the process of reading, analysing and characterizing materials, because it can do this automatically, in a very short time, avoiding the propagation of errors. However, after obtaining the data, in most cases an evaluation of the results is needed.

Automating the evaluation of the obtained data leads to more accurate results and minimizes errors. An optimal environment for such data processing can be the MATLAB language.

MATLAB (from Matrix Laboratory) is a development environment for numerical computation and statistical analysis, it allows manipulation of matrices, visualization of functions, implementation of algorithms, creation of interfaces and can interact with other applications [4].

The focus of the present work is on mechanical static tests performed on composite materials, more precisely on data collection, their processing and finally, obtaining correct data for material characterization. The processing and final data acquisition were performed using an algorithm especially created for this purpose in MATLAB and its functionality is explained in detail in this article.

## 2. Materials and methods

For material testing, the Instron 8852 mechanical testing machine was used, equipped with special modules for each test. The Instron 8850 Series System is a servo-hydraulic, biaxial dynamic testing

THE ANNALS OF "DUNAREA DE JOS" UNIVERSITY OF GALATI
FASCICLE IX. METALLURGY AND MATERIALS SCIENCE
N°. 1 - 2025, ISSN 2668-4748; e-ISSN 2668-4756
Article DOI: https://doi.org/10.35219/mms.2025.1.05

system that provides axial and torsional loads on the specimen. Featuring a precision-aligned, high-rigidity two-column frame, the 8850 series meets the challenging demands of a diverse range of static and dynamic biaxial testing requirements. The Instron 8852 system has an axial load capacity of ±100 kN and a torque capacity of ±1000 Nm with an actuator axial travel of 150 mm and a rotational travel of 90° [5].

The pressure required to operate the mechanical testing machine is provided by the Instron 3520 series hydraulic pump, with a noise level of between 58-63 dB. The pump provides a flow rate ranging from 13 litres/min to 249 litres/min and a nominal operating pressure between 207 bar and 280 bar. The pump is equipped with a programmable logic controller (PLC), which provides system control, monitors oil level and temperature, filter status and engine temperature. Cooling is achieved by using an air-cooling unit, which transfers heat directly to the ambient air [6].

Console software is the main user interface for the 8800MT. Running on a PC, it allows all controller functions to be viewed and configured including control-loop optimization, setting of operational limits, and running of simple cyclic tests. Console provides the foundation for running more demanding tests in application software such as WaveMatrix and Bluehill 3 [7].

For complex data processing, in order to obtain results that reflect as faithfully as possible, the behavior of the tested materials, the Matlab programming language, developed by MathWorks, was used. This tool, through its libraries, allows advanced numerical processing, the implementation of complex algorithms, graphical representation of functions and data, making it the right environment for effective processing and analysis of the data obtained when testing the mechanical characteristics of materials. The MATLAB version used is: 8.4.0.150421 (R2014b). For tensile, compression and bending testing of composite materials, the test methods given by ASTM standards, corresponding to each type of test, were used [8-10].

The software dedicated to the primary processing of the data acquired from the mechanical testing machine, which is used to calculate the characteristic parameters of each test, identifies the critical points on the stress/strain curve, with the conventional tensile test characteristic curve as a benchmark (Fig. 1).

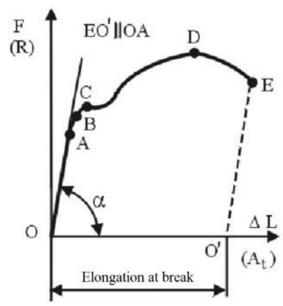


***Fig. 1.*** *The conventional tensile test characteristic curve: OA – quasi-linear zone; OB – elastic zone; C – the horizontal portion starting from point C, called the yield point; D – maximum force; E – breaking point of the specimen*

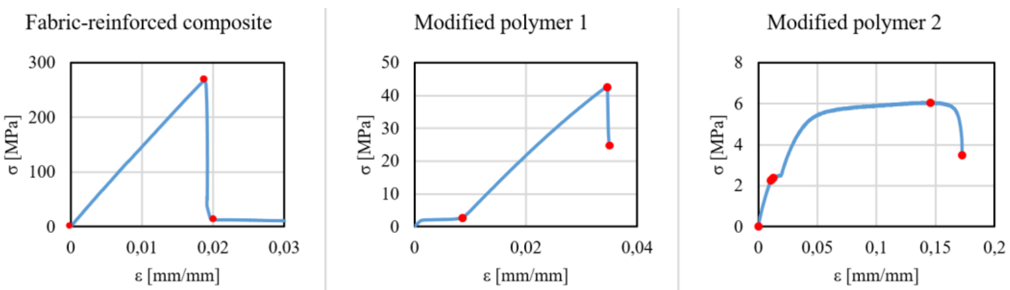


***Fig. 2.*** *Examples of different shapes of curves obtained on the same mechanical testing machine for composite materials, depending on the material class*

Starting from this shape of the conventional characteristic curve, it is easy to identify the technical elasticity limit (segment OA), the area in which the modulus of elasticity is calculated. The technical proportionality limit is the point on the curve corresponding to the maximum normal stress at which the slope of the tangent to the characteristic curve differs by 10% from the slope of the tangent at the origin [11]. In the case of composite materials, depending on the material class, the curves obtained on the same mechanical testing machine may have different or even completely different shapes, as presented in the examples in Figure 2.

In Figure 2, the curve on the left was obtained from a fabric-reinforced composite material, the preparation method being presented in Table 1. The curve in the middle represents the result of the tensile test on Epiphen E 4020 epoxy resin modified with aspartic acid (0.1 mol phr), which was maintained for half an hour after moulding under the influence of electromagnetic radiation (blue-UV). The curve on the right represents the result of the tensile test on SG1452 epoxy resin, modified with (poly)methylene methacrylate (PMMA), also maintained for half an hour after moulding under the influence of electromagnetic radiation (blue-UV).

The shapes of the curves differ, both from the shape of the conventional characteristic curve and from each other. While for the first and last curves, the area of proportionality between force and elongation (OA) is exactly the first part of the curve, for the second curve this area is preceded by a portion of the curve that represents the repositioning of the jaws of the mechanical testing machine. Starting from the figure above and from the way the technical proportionality limit is identified, in the case of the curve (in the middle) the Young's modulus will be calculated based on the initial area of the curve, so an incorrect result will be obtained.

***Table 1.*** *Materials and architecture used to obtain the fabric reinforced composite material*

| Layer | Fabric type | Specific density [g/m$^2$] | Orientation [°] |
|---|---|---|---|
| 1-4 | Mixt (aramid carbon) | 188 | 0/90/0/90 |
| 5-8 | Mixt (aramid carbon) | 68 | 45/-45/45/-45 |
| 9-10 | Carbon | 240 | 0/0 |
| 11-12 | Glass | 108 | 90/90 |
| 13-14 | Glass | 163 | 45/-45 |
| 15-18 | Glass | 280 | 0/0/0/0 |
| 19-20 | Glass | 163 | 45/-45 |
| 21-22 | Glass | 108 | 90/90 |
| 23-28 | Carbon | 160 | 0/0/45/-45/45/-45 |
| 29-30 | Carbon | 240 | 0/0 |

## 3. Results and discussions

Previous experience has shown that results from mechanical tests of composite materials can produce different curve shapes; therefore, the primary processing performed by the software of the mechanical testing machine (Bluehill 3) is not sufficient to obtain realistic results. Therefore, a code was written in the MATLAB programming language, which allows the processing of data obtained from the Instron 8852 universal mechanical testing machine.

The data provided by the mechanical testing machine are obtained in comma-separated values (CSV) format, one file for each tested specimen, similar to the example in Figure 3. According to the method defined in the Bluehill 3 application, in this file, by columns, the data are saved in columns as follows: Time (s), Elongation (mm), Load (N), Specific tensile elongation (mm), Tensile strain (mm/mm) and Tensile stress (MPa).

| | A | B | C | D | E | F |
|---|---|---|---|---|---|---|
| 1 | Time | Elongation | Load | Specific tensile elongation | Tensile strain (Elongation) | Tensile stress |
| 2 | (s) | (mm) | (N) | (mm) | (mm/mm) | (MPa) |
| 3 | 0 | 0,01603 | -0,32846 | -0,00132 | -0,00003 | -0,01141 |
| 4 | 0,1 | 0,02247 | 3,38137 | 0,00512 | 0,0001 | 0,11748 |
| 5 | 0,2 | 0,03034 | 6,94066 | 0,01299 | 0,00026 | 0,24115 |
| 6 | 0,3 | 0,03918 | 10,32148 | 0,02182 | 0,00044 | 0,35861 |
| 7 | 0,4 | 0,0476 | 13,5313 | 0,03025 | 0,0006 | 0,47013 |
| 8 | 0,5 | 0,05558 | 16,34303 | 0,03823 | 0,00076 | 0,56782 |
| 9 | 0,6 | 0,06394 | 18,58927 | 0,04659 | 0,00093 | 0,64586 |
| 10 | 0,7 | 0,07252 | 20,48202 | 0,05517 | 0,0011 | 0,71163 |
| 11 | 0,8 | 0,08084 | 23,31186 | 0,06348 | 0,00127 | 0,80995 |
| 12 | 0,9 | 0,08896 | 26,14528 | 0,07161 | 0,00143 | 0,90839 |
| 13 | 1 | 0,09722 | 28,43645 | 0,07987 | 0,0016 | 0,98799 |
| 14 | 1,1 | 0,10555 | 31,19174 | 0,0882 | 0,00176 | 1,08372 |
| 15 | 1,2 | 0,11388 | 33,64328 | 0,09653 | 0,00193 | 1,1689 |
| 16 | 1,3 | 0,12226 | 36,59449 | 0,10491 | 0,0021 | 1,27144 |
| 17 | 1,4 | 0,13043 | 38,86968 | 0,11308 | 0,00226 | 1,35049 |
| 18 | 1,5 | 0,13891 | 41,52585 | 0,12156 | 0,00243 | 1,44277 |
| 19 | 1,6 | 0,14756 | 44,0269 | 0,1302 | 0,0026 | 1,52967 |
| 20 | 1,7 | 0,15551 | 46,30633 | 0,13815 | 0,00276 | 1,60886 |
| 21 | 1,8 | 0,16375 | 48,2326 | 0,1464 | 0,00293 | 1,67579 |

***Fig. 3.*** *Representative format of mechanical test data automatically produced by the specialized software (Bluehill 3)*

THE ANNALS OF "DUNAREA DE JOS" UNIVERSITY OF GALATI
FASCICLE IX. METALLURGY AND MATERIALS SCIENCE
N°. 1 - 2025, ISSN 2668-4748; e-ISSN 2668-4756
Article DOI: https://doi.org/10.35219/mms.2025.1.05

For *n* tested materials, each with *m* samples, there will be *n*m* CSV files. These files are grouped into *n* folders, each material in its own folder, named after the material.

The algorithm created in MATLAB (Annex 1) for processing these data goes through several stages, as follows:

1. reads all CSV files from the existing folders;
2. identifies and extracts the columns with strain and stress data;
3. saves the extracted data in an Excel file in the "Original data" sheet (optionally, a graphical representation of the curves for each material can be generated manually using the saved data – Fig. 4);

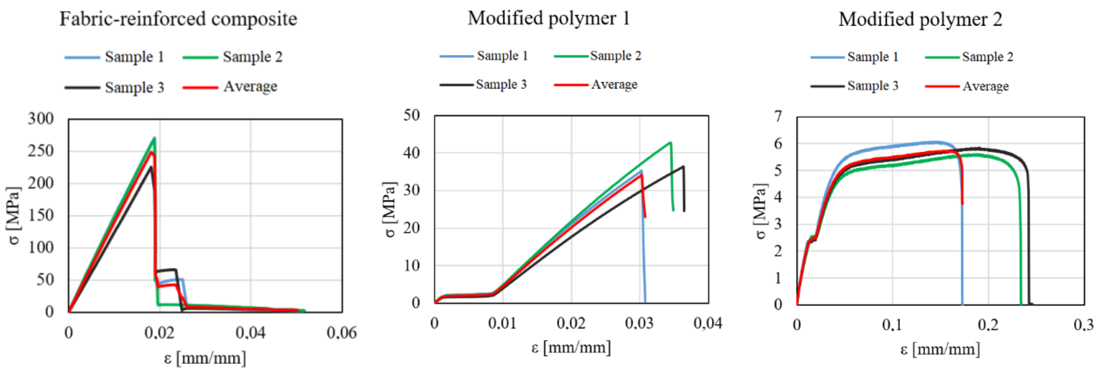


***Fig. 4.*** *Graphics obtained immediately after mechanical testing*

4. using the moving average method, the algorithm calculates the values of the trend curve;
5. the length of the data series recorded following the performed tests is adjusted (depending on the duration of the test, the data series for different tests may vary);
6. saves the new values in the same Excel file, in the "ALL processed curves" sheet;
7. automatically generates a graphic for each material, with redrawn curves (Fig. 5);
8. allows manual selection on the graph of the area on which the modulus of elasticity is to be calculated (Fig. 6);

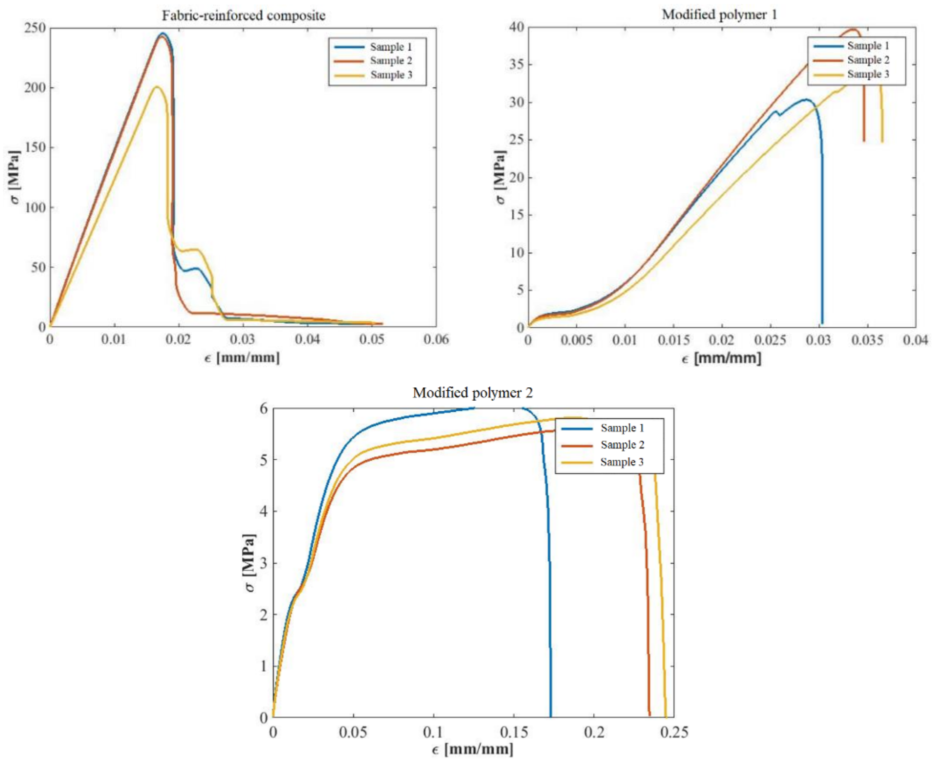


***Fig. 5.*** *Graphics obtained automatically by the algorithm, after adjusting the lengths of all vectors to the minimum length identified*

THE ANNALS OF “DUNAREA DE JOS” UNIVERSITY OF GALATI
FASCICLE IX. METALLURGY AND MATERIALS SCIENCE
N°. 1 - 2025, ISSN 2668-4748; e-ISSN 2668-4756
Article DOI: https://doi.org/10.35219/mms.2025.1.05

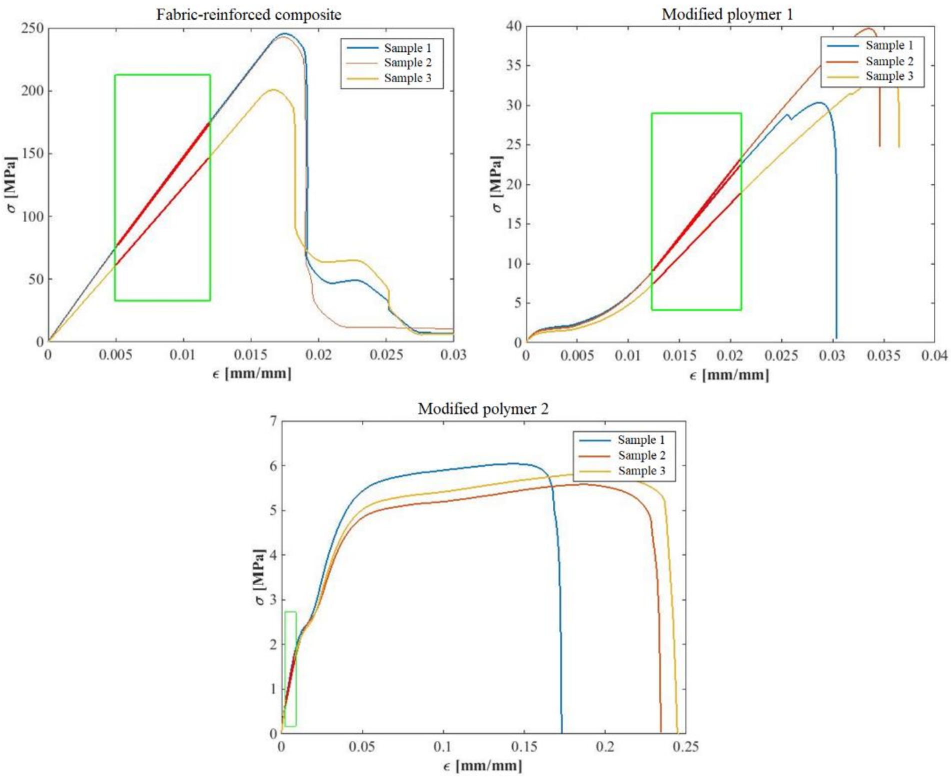


***Fig. 6.*** *Manual selection, on the graph, of the area on which the modulus of elasticity is to be calculated*

9. draws the tangent to each curve on the graph, within the selected area;
10. saves the values of the slopes of all curves in the Excel file, in the sheet "ALL Slopes" (Table 2);
11. identifies the values of the slopes that deviate by more than 5% from the average and eliminates the slopes of the respective curves;
12. calculates the average of the remaining slopes and their standard deviation;
13. saves the remaining slopes in the Excel file, in the sheet "GOOD and AVERAGE Slopes" (Table 3);
14. allows manual selection of the portion of the curves that includes the area of interest;
15. saves the new curves in the Excel file, in the sheet "Final Curves" (automatically generates the final shapes of the curves for all materials – Fig. 7);
16. calculates the average curve, for each material;
17. saves in the Excel file, in the sheet "AVERAGE Curves", the data representing the average curves of the materials.

***Table 2.*** *Values of the slopes of all curves, automatically calculated by the algorithm*

| | **$SE_1$ [Mpa]** | **$SE_2$ [Mpa]** | **$SE_3$ [Mpa]** |
|---|---|---|---|
| **Fabric-reinforced composite** | 14510 | 14382 | 12398 |
| **Modified polymer 1** | 1563 | 1653 | 1339 |
| **Modified polymer 2** | 205 | 180 | 192 |

***Table 3.*** *Values of the slopes of all curves, automatically calculated by the algorithm for the remaining slopes, after eliminating the ones with a deviation greater than 5%*

| | **$SE_1$ [Mpa]** | **$SE_2$ [Mpa]** | **$SE_3$ [Mpa]** | **Average [MPa]** | **St. dev.** |
|---|---|---|---|---|---|
| **Fabric-reinforced composite** | 14510 | 14382 | - | 14446 | 64 |
| **Modified polymer 1** | 1563 | 1653 | - | 1608 | 45 |
| **Modified polymer 2** | 205 | 180 | 192 | 192 | 10.20 |

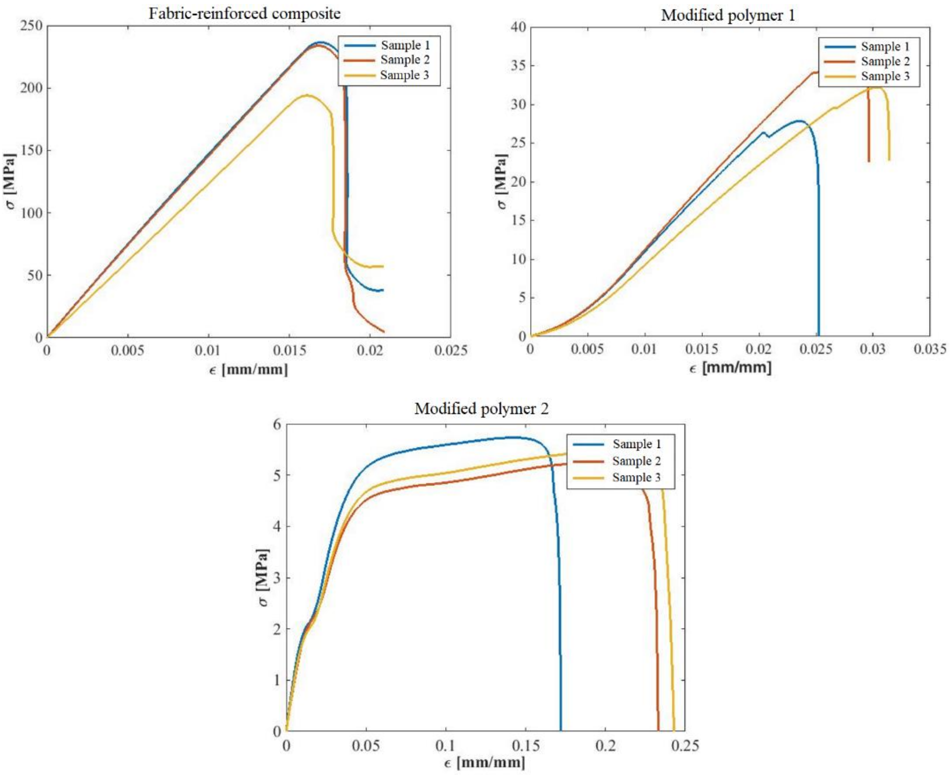


***Fig. 7.** Final shapes of the curves automatically represented by the algorithm for each mechanically tested material*

These final results are visibly much closer to a conventional curve, the average values of the monitored parameters being calculated on the average curve - a curve that best reproduces the shape of the closest curve, after the curves with a slope deviating more than 5% from the average have been eliminated (comparison: original vs. processed with MATLAB).

The algorithm proposed in this work calculates the slope and the longitudinal modulus of elasticity (Young's modulus) over the manually selected interval. Also, provides both the elastic modulus values for all curves, as well as the relevant values and their average, as seen in Table 3.

These extra steps and the proposed algorithm provide the foundation to rapidly and elegantly avoid some possible errors that can interfere with the mechanical testing results, especially when analysing composite materials.

## 4. Conclusions

The multitude of composite materials obtained through an increasing number of combinations of components can create situations that are difficult to manage in relation to results from the necessary testing of these materials. The automation of data processing is nothing new in the area of materials analysis and its utilisation in the present work comes with an optimisation tailored to the particularities of the aforementioned composite materials. Thus, this paper has demonstrated that the addition of some steps in an algorithm used for data processing of mechanical testing results can ensure greater reliability through elimination of possible errors that can appear during the initial processing of data. The demonstration was carried out using selected composite materials that presented significant differences both among themselves and compared to conventional materials.

Although the whole process still needs an operator to select an area on the obtained curves to be used in the calculation process, the much higher precision of the final results makes this process viable.

## References

**[1]. Carey J. P.**, *Introduction to braided composites*, *Handbook of Advances in Braided Composite Materials: Theory, Production, Testing and Applications*, p. 1-21, doi: 10.1016/B978-0-08-100369-5.00001-5, Jan. 2017.

**[2]. *****, *Mechanical Testing Methods | Anton Paar Wiki*, [Online]. Available: https://wiki.anton-paar.com/en/mechanical-testing-methods/, Accessed: Apr. 09, 2025.

**[3]. *****, *Mechanical Testing of Composites*, [Online]. Available: https://www.addcomposites.com/post/mechanical-testing-of-composites, Accessed: Apr. 09, 2025.

N°. 1 - 2025, ISSN 2668-4748; e-ISSN 2668-4756
Article DOI: https://doi.org/10.35219/mms.2025.1.05

**[4].** ***, *MATLAB*, [Online]. Available: https://www.mathworks.com/products/matlab.html, Accessed: Apr. 09, 2025.
**[5].** ***, *8850 SERIES AXIAL-TORSION SYSTEM ±100 kN, ±1000 Nm / ±250 kN, ±2000 Nm*, 2024, [Online]. Available: www.instron.com, Accessed: Apr. 09, 2025.
**[6].** ***, *Hydraulic Power Unit 3621 Series (207 Bar)*, 2024, [Online]. Available: www.instron.com, Accessed: Apr. 09, 2025.
**[7].** ***, *8800MT CONTROLLER Intelligence and safety built in*, 2023, [Online]. Available: www.instron.com, Accessed: Apr. 09, 2025.
**[8].** ***, *Designation: D3039/D3039M − 08 Standard Test Method for Tensile Properties of Polymer Matrix Composite Materials 1*, doi: 10.1520/D3039_D3039M-08, 2008.
**[9].** ***, *Standard Test Method for Flexural Properties of Polymer Matrix Composite Materials 1*, doi: 10.1520/D7264_D7264M-21, 2008.
**[10].** ***, *Standard Practice Unnotched Compression Testing of Polymer Matrix Composite Laminates 1*, doi: 10.1520/D8066_D8066M, 2023.
**[11]. Mocanu Costel Iulian**, *Rezistența materialelor*, 2nd ed. Galati: Zigotto, 2005.

THE ANNALS OF "DUNAREA DE JOS" UNIVERSITY OF GALATI
FASCICLE IX. METALLURGY AND MATERIALS SCIENCE
N°. 1 - 2025, ISSN 2668-4748; e-ISSN 2668-4756
Article DOI: https://doi.org/10.35219/mms.2025.1.05

## Annex 1

```
clear all;
clc;

selectedFolder = uigetdir('', 'Select a folder');
if isempty(selectedFolder)
   disp('Selection canceled.');
else
   subdirectories = dir(selectedFolder);
   subdirectories =
subdirectories(~ismember({subdirectories.name}, {'.', '..'}) &
[subdirectories.isdir]);
   if isempty(subdirectories)
      disp('Warning: No subdirectories found.');
   else
   end
lungimiVectoriEpsilon = [];
end
      for i = 1:length(subdirectories)
         currentName = subdirectories(i).name;
         currentSubdirectory = fullfile(selectedFolder,
currentName);
         NumeSubdirector = strtok(subdirectories(i).name, '.');
         csvFiles = dir(fullfile(currentSubdirectory, '*.csv'));
         if ~isempty(csvFiles)
            for j = 1:length(csvFiles)
               currentCSVFile = fullfile(currentSubdirectory,
csvFiles(j).name);
               tableData = readtable(currentCSVFile, 'Delimiter', ';');
               epsilonColumnIndex =
findColumnByPartialName(tableData.Properties.VariableNames,
'Deform');
               sigmaColumnIndex =
findColumnByPartialName(tableData.Properties.VariableNames,
'Stress');
               if ~isempty(epsilonColumnIndex) &&
~isempty(sigmaColumnIndex)
                  epsilonColumn = str2double(strrep(tableData{:,
epsilonColumnIndex}, ',', '.'));
                  sigmaColumn = str2double(strrep(tableData{:,
sigmaColumnIndex}, ',', '.'));
                  epsilonColumn =
epsilonColumn(~isnan(epsilonColumn));
                  sigmaColumn =
sigmaColumn(~isnan(sigmaColumn));
                  epsilonColumn = abs(epsilonColumn);
                  sigmaColumn = abs(sigmaColumn);
                  lungimiVectoriEpsilon = [lungimiVectoriEpsilon;
length(epsilonColumn)];
                  grupuriCaractere = strsplit(NumeSubdirector, ' ');
                  ultimulGrup = grupuriCaractere{end};
                  epsilonColumnName =
matlab.lang.makeValidName(['Epsilon_' ultimulGrup '_'
num2str(j)]);
                  sigmaColumnName =
matlab.lang.makeValidName(['Sigma_' ultimulGrup '_'
num2str(j)]);
                  epsilonColumnNames{i}{j} =
epsilonColumnName;
                  sigmaColumnNames{i}{j} = sigmaColumnName;
                  validNameEpsilon =
matlab.lang.makeValidName(['Epsilon_' ultimulGrup '_'
num2str(j)]);
                  validNameSigma =
matlab.lang.makeValidName(['Sigma_' ultimulGrup '_'
num2str(j)]);
                  assignin('base', validNameEpsilon, epsilonColumn);
                  assignin('base', validNameSigma, sigmaColumn);
                  disp(['Storing the epsilon vector for'
validNameEpsilon ' and the sigma vector for ' validNameSigma ' in
workspace.']);
               else
                  disp(['Worning: The columns for Deformation or
Stress were not found in the file header.']);
               end
            end
         end
         nameBeforeDot = strtok(currentName, '.');
         disp(['The sigma and epsilon vectors for the directory '
nameBeforeDot ' were saved in the workspace.']);
      end

dataCell = cell(length(epsilonColumnNames) * 2, 2);
idx = 1;
for i = 1:length(epsilonColumnNames)
   for j = 1:length(epsilonColumnNames{i})
      epsilonVarName = epsilonColumnNames{i}{j};
      sigmaVarName = sigmaColumnNames{i}{j};
      epsilonData = evalin('base', epsilonVarName);
      sigmaData = evalin('base', sigmaVarName);
      dataCell{idx, 1} = epsilonVarName;
      dataCell{idx, 2} = epsilonData;
      dataCell{idx+1, 1} = sigmaVarName;
      dataCell{idx+1, 2} = sigmaData;
      idx = idx + 2;
   end
end

allData = cell2table(dataCell, 'VariableNames', {'Nume',
'Termenul'});
[~, folderName, ~] = fileparts(selectedFolder);
excelFileName = fullfile(selectedFolder, [folderName '.xlsx']);
writetable(allData, excelFileName, 'Sheet', 'Date originale',
'WriteVariableNames', true);
disp(['Datele au fost salvate in fisierul Excel: ' excelFileName]);

windowSize = 60;
for i = 1:length(subdirectories)
   currentName = subdirectories(i).name;
   currentSubdirectory = fullfile(selectedFolder, currentName);
   figure('Name', currentName);
   for j = 1:length(epsilonColumnNames{i})
      epsilonVarName = epsilonColumnNames{i}{j};
      sigmaVarName = sigmaColumnNames{i}{j};
      epsilonData = evalin('base', epsilonVarName);
      sigmaData = evalin('base', sigmaVarName);
      epsilonSmoothed = smooth(epsilonData, windowSize);
      sigmaSmoothed = smooth(sigmaData, windowSize);
      assignin('base', sigmaVarName, sigmaSmoothed);
      plot(epsilonSmoothed, sigmaSmoothed, 'DisplayName',
['Sample ' num2str(j)]);
      hold on;
   end
   title(['Curves ' strtok(currentName, '.')]);
   xlabel('\epsilon [mm/mm]');
   ylabel('\sigma [MPa]');
   legend('show');
saveas(gcf, fullfile(selectedFolder, ['Curves ' currentName '.jpg']));
   close all
end

minLength = min(lungimiVectoriEpsilon);
for i = 1:length(epsilonColumnNames)
   for j = 1:length(epsilonColumnNames{i})
      epsilonVarName = epsilonColumnNames{i}{j};
      sigmaVarName = sigmaColumnNames{i}{j};
      epsilonData = evalin('base', epsilonVarName);
      sigmaData = evalin('base', sigmaVarName);
```

THE ANNALS OF "DUNAREA DE JOS" UNIVERSITY OF GALATI
FASCICLE IX. METALLURGY AND MATERIALS SCIENCE
N°. 1 - 2025, ISSN 2668-4748; e-ISSN 2668-4756
Article DOI: https://doi.org/10.35219/mms.2025.1.05

```
        fEpsilon = @(x) interp1((1:length(epsilonData))', epsilonData, x, 'linear', 'extrap');
        fSigma = @(x) interp1((1:length(sigmaData))', sigmaData, x, 'linear', 'extrap');
        epsilonAdjusted = fEpsilon(linspace(1, length(epsilonData), minLength));
        sigmaAdjusted = fSigma(linspace(1, length(sigmaData), minLength));
        assignin('base', epsilonVarName, epsilonAdjusted);
        assignin('base', sigmaVarName, sigmaAdjusted);
    end
end

for i = 1:length(subdirectories)
    currentName = subdirectories(i).name;
    NumeCurent = strtok(currentName, '.');
    grupuriCaractere = strsplit(NumeCurent, ' ');
    ultimulGrup = grupuriCaractere{end};
    figure('Name', ultimulGrup);
    for j = 1:length(epsilonColumnNames{i})
        epsilonVarName = epsilonColumnNames{i}{j};
        sigmaVarName = sigmaColumnNames{i}{j};
        epsilonData = evalin('base', epsilonVarName);
        sigmaData = evalin('base', sigmaVarName);
        plot(epsilonData, sigmaData, 'DisplayName', ['Sample ' num2str(j)]);
        hold on;
    end
    title(['Curves ' strtok(currentName, '.')]);
    xlabel('\epsilon [mm/mm]');
    ylabel('\sigma [MPa]');
    legend('show');
    disp(['Select border for SLOPES, on the graph ' strtok(currentName, '.') '.']);
    [xSelected, ySelected] = ginput(2);
    hold on;
    plot(xSelected([1 2 2 1 1]), ySelected([1 1 2 2 1]), 'g-', 'LineWidth', 1);
    intervalX = sort(xSelected);
    intervalY = sort(ySelected);
    validVarNameX = matlab.lang.makeValidName(['Interval_X_' strtok(currentName, '.')]);
    validVarNameY = matlab.lang.makeValidName(['Interval_Y_' strtok(currentName, '.')]);
    assignin('base', validVarNameX, intervalX);
    assignin('base', validVarNameY, intervalY);
     NumeSubdirector = strtok(subdirectories(i).name, '.');
     grupuriCaractere = strsplit(NumeSubdirector, ' ');
     ultimulGrup = grupuriCaractere{end};
    numePanteVector = ['Slopes_' matlab.lang.makeValidName(ultimulGrup)];
    eval([numePanteVector ' = [];']);
    Pante = [];
    for j = 1:length(epsilonColumnNames{i})
        epsilonVarName = epsilonColumnNames{i}{j};
        sigmaVarName = sigmaColumnNames{i}{j};
        epsilonData = evalin('base', epsilonVarName);
        sigmaData = evalin('base', sigmaVarName);
        idxInterval = epsilonData >= intervalX(1) & epsilonData <= intervalX(2);
        epsilonInterval = epsilonData(idxInterval);
        sigmaInterval = sigmaData(idxInterval);
        [~, idx1] = min((epsilonInterval - intervalX(1)).^2 + (sigmaInterval - intervalY(1)).^2);
        [~, idx2] = min((epsilonInterval - intervalX(2)).^2 + (sigmaInterval - intervalY(2)).^2);
        closestX = epsilonInterval([idx1, idx2]);
        closestY = sigmaInterval([idx1, idx2]);
        p = polyfit(closestX, closestY, 1);
        dreaptaTendinta = polyval(p, epsilonInterval);
        panta = p(1);
        disp(panta)
        eval([numePanteVector ' = [ ' numePanteVector ' slope]']);
        validCurrentName = matlab.lang.makeValidName(currentName);
        fieldName = matlab.lang.makeValidName(['Sample_' num2str(j)]);
        rezultate.(validCurrentName).(fieldName).dreaptaTendinta = dreaptaTendinta;
        rezultate.(validCurrentName).(fieldName).panta = panta;
        plot(epsilonInterval, dreaptaTendinta, 'r', 'LineWidth', 1, 'DisplayName', ['Right Samples ' num2str(j)]);
    end
saveas(gcf, fullfile(selectedFolder, ['Slopes ' ultimulGrup '.jpg']));
end

disp('SLOPE results have been calculated and displayed..');
for i = 1:length(subdirectories)
    currentName = subdirectories(i).name;
    currentSubdirectory = fullfile(selectedFolder, currentName);
    figure('Name', currentName);
    for j = 1:length(epsilonColumnNames{i})
        epsilonVarName = epsilonColumnNames{i}{j};
        sigmaVarName = sigmaColumnNames{i}{j};
        epsilonData = evalin('base', epsilonVarName);
        sigmaData = evalin('base', sigmaVarName);
        plot(epsilonData, sigmaData, 'LineWidth', 2, 'DisplayName', ['Epruveta ' num2str(j)]);
        hold on;
    end
    title(['Curves ' strtok(currentName, '.')]);
    xlabel('\epsilon [mm/mm]');
    ylabel('\sigma [MPa]');
    legend('show');
    disp(['Select the CURVE AREA you want to represent, on the graph ' strtok(currentName, '.') '.']);
    [xSelected, ySelected] = ginput(2);
    for j = 1:length(epsilonColumnNames{i})
        epsilonVarName = epsilonColumnNames{i}{j};
        sigmaVarName = sigmaColumnNames{i}{j};
        epsilonData = evalin('base', epsilonVarName);
        sigmaData = evalin('base', sigmaVarName);
        idxChenar = epsilonData >= min(xSelected) & epsilonData <= max(xSelected) & sigmaData >= min(ySelected) & sigmaData <= max(ySelected);
        epsilonDataNou = epsilonData(idxChenar);
        sigmaDataNou = sigmaData(idxChenar);
        epsilonDataNou = epsilonDataNou - epsilonDataNou(1);
        sigmaDataNou = sigmaDataNou - sigmaDataNou(1);
        assignin('base', epsilonVarName, epsilonDataNou);
        assignin('base', sigmaVarName, sigmaDataNou);
        plot(epsilonDataNou, sigmaDataNou, 'r', 'LineWidth', 2, 'DisplayName', ['Sample ' num2str(j)]);
    end
end

noiLungimiVectoriEpsilon = [];
for i = 1:length(epsilonColumnNames)
    for j = 1:length(epsilonColumnNames{i})
        epsilonVarName = epsilonColumnNames{i}{j};
        epsilonData = evalin('base', epsilonVarName);
        noiLungimiVectoriEpsilon = [noiLungimiVectoriEpsilon; length(epsilonData)];
    end
end

nouaMinLength = min(noiLungimiVectoriEpsilon);
for i = 1:length(epsilonColumnNames)
    for j = 1:length(epsilonColumnNames{i})
        epsilonVarName = epsilonColumnNames{i}{j};
        sigmaVarName = sigmaColumnNames{i}{j};
        epsilonData = evalin('base', epsilonVarName);
```

N°. 1 - 2025, ISSN 2668-4748; e-ISSN 2668-4756
Article DOI: https://doi.org/10.35219/mms.2025.1.05

```
        sigmaData = evalin('base', sigmaVarName);
        fEpsilon = @(x) interp1((1:length(epsilonData))', epsilonData,
x, 'linear', 'extrap');
        fSigma = @(x) interp1((1:length(sigmaData))', sigmaData, x,
'linear', 'extrap');
        epsilonAdjusted = fEpsilon(linspace(1, length(epsilonData),
nouaMinLength));
        sigmaAdjusted = fSigma(linspace(1, length(sigmaData),
nouaMinLength));
        assignin('base', epsilonVarName, epsilonAdjusted);
        assignin('base', sigmaVarName, sigmaAdjusted);
    end
end

datePrelucrateCell = cell(length(epsilonColumnNames) * 2, 2);
idx = 1;
for i = 1:length(epsilonColumnNames)
    for j = 1:length(epsilonColumnNames{i})
        epsilonVarName = epsilonColumnNames{i}{j};
        sigmaVarName = sigmaColumnNames{i}{j};
        epsilonData = evalin('base', epsilonVarName);
        sigmaData = evalin('base', sigmaVarName);
        datePrelucrateCell{idx, 1} = epsilonVarName;
        datePrelucrateCell{idx, 2} = epsilonData;
        datePrelucrateCell{idx+1, 1} = sigmaVarName;
        datePrelucrateCell{idx+1, 2} = sigmaData;
        idx = idx + 2;
    end
end
toateDatelePrelucrate = cell2table(datePrelucrateCell,
'VariableNames', {'Name', 'Term'});
writetable(toateDatelePrelucrate, excelFileName, 'Sheet', 'Curves
processed ALL ', 'WriteVariableNames', true, 'Range', 'A1');
disp(['The processed data (Epsilon and Sigma) were saved in the
Excel file: ' excelFileName]);
panteCell = cell(length(subdirectories), 2);
for i = 1:length(subdirectories)
    currentName = subdirectories(i).name;
      NumeSubdirector = strtok(subdirectories(i).name, '.');
      grupuriCaractere = strsplit(NumeSubdirector, ' ');
      ultimulGrup = grupuriCaractere{end};
    numePanteVector = ['Slopes_'
matlab.lang.makeValidName(ultimulGrup)];
    valoriPante = evalin('base', numePanteVector);
    panteCell{i, 1} = numePanteVector;
    panteCell{i, 2} = valoriPante;
end
tabelPante = cell2table(panteCell, 'VariableNames', {'Name',
'Slope'});
writetable(tabelPante, excelFileName, 'Sheet', 'ALL slopes',
'WriteVariableNames', true, 'Range', 'A1');
disp([' The slope values were saved in the Excel file.: '
excelFileName]);
for i = 1:length(subdirectories)
    NumeSubdirector = strtok(subdirectories(i).name, '.');
    grupuriCaractere = strsplit(NumeSubdirector, ' ');
    ultimulGrup = grupuriCaractere{end};
    numePanteVector = ['Slopes_'
matlab.lang.makeValidName(ultimulGrup)];
    numeEpsilonVector = ['Epsilon_'
matlab.lang.makeValidName(ultimulGrup)];
    numeSigmaVector = ['Sigma_'
matlab.lang.makeValidName(ultimulGrup)];
    valoriPante = evalin('base', numePanteVector);
    PantaMedie=mean(valoriPante);
    limitaDiferentaRelativa = (PantaMedie*5)/100;
        i = 1;
        pantaEliminata = 0;
        while i < length(valoriPante)
            difRelative = abs(mean(valoriPante) - valoriPante(i));
            if difRelative > limitaDiferentaRelativa
                valoriPante(i) = [];
               pantaEliminata = i;
            else
                i = i + 1;
            end
        end
    assignin('base', numePanteVector, valoriPante);
    if pantaEliminata > 0
        numeEpsilonEliminat = ['Epsilon_'
matlab.lang.makeValidName(ultimulGrup) '_'
num2str(pantaEliminata)];
        numeSigmaEliminat = ['Sigma_'
matlab.lang.makeValidName(ultimulGrup) '_'
num2str(pantaEliminata)];
        evalin('base', ['clear ' numeEpsilonEliminat ' '
numeSigmaEliminat]);
    end
end
     assignin('base', numePanteVector, valoriPante);
mediiPanteCell = cell(length(subdirectories), 3);
for i = 1:length(subdirectories)
    currentName = strsplit(strtok(subdirectories(i).name, '.'));
    ultimulGrup = currentName{end};
    numePanteVector = ['Slopes_'
matlab.lang.makeValidName(ultimulGrup)];
    valoriPante = evalin('base', numePanteVector);
    mediaPantelor = mean(valoriPante);
     mediiPanteCell{i, 1} = ultimulGrup;
    mediiPanteCell{i, 2} = valoriPante;
    mediiPanteCell{i, 3} = mediaPantelor;
end
tabelMediiPante = cell2table(mediiPanteCell, 'VariableNames',
{'Subdirectory', 'Slope', 'Slopes_average'});
writetable(tabelMediiPante, excelFileName, 'Sheet', 'GOOD and
AVERAGE slopes', 'WriteVariableNames', true, 'Range', 'A1');
disp(['SIGNIFICANT slopes and their means were saved in the
Excel file: ' excelFileName]);
datePrelucrateCell = cell(length(epsilonColumnNames) * 2, 2);
idx = 1;
for i = 1:length(epsilonColumnNames)
    for j = 1:length(epsilonColumnNames{i})
        epsilonVarName = epsilonColumnNames{i}{j};
        sigmaVarName = sigmaColumnNames{i}{j};
        try
            epsilonData = evalin('base', epsilonVarName);
            sigmaData = evalin('base', sigmaVarName);
            datePrelucrateCell{idx, 1} = epsilonVarName;
            datePrelucrateCell{idx, 2} = epsilonData;
            datePrelucrateCell{idx+1, 1} = sigmaVarName;
            datePrelucrateCell{idx+1, 2} = sigmaData;
            idx = idx + 2;
        catch
            disp(['Vector ' epsilonVarName ' or ' sigmaVarName ' was
not found in the workspace. Moving on to the next vector.']);
        end
    end
end
toateDatelePrelucrate = cell2table(datePrelucrateCell,
'VariableNames', {'Name', 'Term'});
writetable(toateDatelePrelucrate, excelFileName, 'Sheet', 'Curves
FINAL', 'WriteVariableNames', true, 'Range', 'A1');
disp(['FINAL curves (Epsilon and Sigma) were saved in the Excel
file: ' excelFileName]);

epsilonMediu = zeros(length(subdirectories),
length(epsilonAdjusted));
sigmaMediu = zeros(length(subdirectories),
length(epsilonAdjusted));
for i = 1:length(subdirectories)
    NumeSubdirector = strtok(subdirectories(i).name, '.');
    grupuriCaractere = strsplit(NumeSubdirector, ' ');
```

```
    ultimulGrup = grupuriCaractere{end};
    numarVectori = 0;
    for j = 1:sigmaColumnIndex
        numeEpsilonVector = ['Epsilon_'
matlab.lang.makeValidName(ultimulGrup) '_' num2str(j)];
        numeSigmaVector = ['Sigma_'
matlab.lang.makeValidName(ultimulGrup) '_' num2str(j)];
        if evalin('base', ['exist(''' numeEpsilonVector ''', ''var'')']) &&
evalin('base', ['exist(''' numeSigmaVector ''', ''var'')'])
            epsilonVector = evalin('base', numeEpsilonVector);
            sigmaVector = evalin('base', numeSigmaVector);
            epsilonMediu(i, :) = epsilonMediu(i, :) + epsilonVector;
            sigmaMediu(i, :) = sigmaMediu(i, :) + sigmaVector;
            numarVectori = numarVectori + 1;
        else
            disp(['Vector ' numeEpsilonVector ' or ' numeSigmaVector '
was not found in the workspace. Moving on to the next vector.']);
        end
    end
    if numarVectori > 0
        epsilonMediu(i, :) = epsilonMediu(i, :) / numarVectori;
        sigmaMediu(i, :) = sigmaMediu(i, :) / numarVectori;
        epsilonSubdirectorCell{i} = epsilonMediu(i, :);
        sigmaSubdirectorCell{i} = sigmaMediu(i, :);
        numeMedieEpsilon = ['Epsilon_AVERAGE_'
matlab.lang.makeValidName(ultimulGrup)];
        numeMedieSigma = ['Sigma_AVERAGE_'
matlab.lang.makeValidName(ultimulGrup)];
        assignin('base', numeMedieEpsilon, epsilonMediu(i, :));
        assignin('base', numeMedieSigma, sigmaMediu(i, :));
    else
        disp(['There are no vectors for the subdirectory '
NumeSubdirector '. Moving on to the next subdirectory.']);
    end
end

toateMediileCell = cell(length(subdirectories), 2);
idx = 1;
for i = 1:length(subdirectories)
    NumeSubdirector = strtok(subdirectories(i).name, '.');
    grupuriCaractere = strsplit(NumeSubdirector, ' ');
    ultimulGrup = grupuriCaractere{end};
    numeMedieEpsilon = ['Epsilon_AVERAGE_'
matlab.lang.makeValidName(ultimulGrup)];
    numeMedieSigma = ['Sigma_AVERAGE_'
matlab.lang.makeValidName(ultimulGrup)];
    try
        epsilonMediu = evalin('base', numeMedieEpsilon);
        sigmaMediu = evalin('base', numeMedieSigma);
        toateMediileCell{idx, 1} = numeMedieEpsilon;
        toateMediileCell{idx, 2} = epsilonMediu;
        toateMediileCell{idx+1, 1} = numeMedieSigma;
        toateMediileCell{idx+1, 2} = sigmaMediu;
        idx = idx + 2;
    catch
        disp(['Averages for the subdirectory ' NumeSubdirector ' were
not found in the workspace. Moving to the next subdirectory.']);
    end
end

toateMediile = cell2table(toateMediileCell, 'VariableNames',
{'Name', 'Average'});
writetable(toateMediile, excelFileName, 'Sheet', 'AVERAGE
Curves', 'WriteVariableNames', true, 'Range', 'A1');
disp(['Epsilon and Sigma AVERAGES were saved in the Excel
file: ' excelFileName]);
```

THE ANNALS OF "DUNAREA DE JOS" UNIVERSITY OF GALATI
FASCICLE IX. METALLURGY AND MATERIALS SCIENCE
N°. 1 - 2025, ISSN 2668-4748; e-ISSN 2668-4756
Article DOI: https://doi.org/10.35219/mms.2025.1.06

# PULMONARY TRAUMA AND PATIENT ACCOMMODATION WITH MECHANICAL VENTILATION - RISE TIME SETTINGS

**Dumitru Adrian DRAGHICI, Angela REPANOVICI**
Transilvania University Brasov, Romania
e-mail: dumitru.draghici@unitbv.ro, arepanovici@unitbv.ro

## ABSTRACT

*The inspiratory rise time in mechanical ventilation refers to the rate at which airway pressure reaches the set target during inspiration. When appropriately adjusted, it enhances patient-ventilator synchrony and improves comfort by increasing the tolerance of ventilator support. However, an excessively rapid rise time may result in elevated airway pressures and abrupt gas delivery, potentially contributing to lung injury or increased patient effort. An inverse correlation exists between rise time and the mechanical work of breathing, such that a shorter rise time is associated with a disproportionately increased in respiratory workload. As the intensity of respiratory effort and duration of mechanical ventilation increase, so does the risk of ventilator-associated lung injury (VALI). It is therefore imperative that ventilator manufacturers incorporate adjustable rise time parameters and corresponding time intervals into their devices to allow precise, individualized ventilator settings that minimize the risk of iatrogenic lung injury.*

KEYWORDS: mechanical ventilation, rise time, pressure, lung trauma, ventilation synchronization

## 1. Introduction

A comprehensive analysis of the current literature in mechanical ventilation and critical care reveals significant insights into ventilatory strategies and their impact on patient outcomes. Several studies have addressed the role of inspiratory cycle termination and rise time settings, with Chiumello *et al.* demonstrating their influence on patient comfort and the risk of ventilator-induced lung injury (VILI) [1, 2]. In efforts to reduce pulmonary overdistension, Kallet et al. advocated for the implementation of low tidal volume ventilation protocols [3], while Simonis et al. evaluated their applicability in patients without acute respiratory distress syndrome (ARDS) [4].

Research into long-term mechanical ventilation has been expanded by Sison et al., who analysed mortality predictors and care determinants in chronically ventilated patients [5], and Donahoe, who explored the economic and logistical challenges associated with prolonged mechanical support [6]. In the context of the COVID-19 pandemic, studies by Bhatraju *et al.*, Guan *et al.*, Wang *et al.*, and Yang *et al.* provide critical data on the clinical characteristics and prolonged ventilatory requirements of patients with severe SARS-CoV-2 infection [7–10]. Studies such as those by Bhatraju *et al.*, Guan *et al.*, Wang *et al.*, and Yang *et al.* investigate clinical characteristics and the extended need for mechanical ventilation in severe COVID-19 cases [7-9].

Additionally, McGrath *et al.* present international, multidisciplinary guidelines for safely conducting tracheostomies in COVID-19 patients, reflecting a shift toward standardized procedural safety [11]. Collectively, this body of literature underscores the necessity of individualized ventilator settings tailored to patient-specific physiology, with the goal of enhancing clinical outcomes and minimizing the risk of iatrogenic lung injury.

With advancements in mechanical ventilation technology, modern ventilators now allow clinicians to adjust the inspiratory rise time – defined as the duration required to reach the preset airway pressure - as well as the criteria for terminating inspiration during pressure support ventilation. This study investigates the physiological impact of short versus long inspiratory rise times by analysing their effects on mechanical work, disconnection thresholds, breathing patterns, and patient comfort. The evolution of ventilator design presents significant challenges in both clinical training and the development of reliable mechatronic systems [1]. Ventilator associated lung injury (VALI) can arise from either suboptimal design or inappropriate ventilator settings. The influence of rise time on mechanical load and VALI is quantified through the dynamic mechanical power equation (MP_dyn), which represents the total energy delivered to the lungs per breath automatically calculated by the ventilator as an indicator of mechanical work. Comparing different rise time settings, it was observed that at a constant pressure, a rise time of 10 ms causes a doubling of the mechanical work compared to a rise time of 300 ms. In the context of prolonged mechanical ventilation (over 12 hours), medical bioengineering guidelines recommend using a rise time of at least 250-300 ms, to significantly reduce the mechanical work imposed on the patient and, implicitly, the risk of ventilator-induced lung injury (VALI). In addition, in the case of non-invasive ventilation (NiV), where comfort and patient-ventilator synchronization are essential, a rise time of 350–400 ms is preferentially recommended, to facilitate patient accommodation and optimize therapy efficiency [2].

## 2. Materials and Methods

The evaluation was performed by comparing the mechanical work displayed by the mechanical ventilator with mathematically calculated mechanical work actually employed by the mechanical ventilation procedure.

Equipment Used: Mechanical Ventilator + test lung.

Mechanical Ventilator: The model used in the experimental tests chosen was the Bellavista 1000-VYARIE, featuring capabilities such as: auto triggering, expiratory pressure safety, hiFlow, rise time adjustment, and support for neonates, paediatric, and adult patients over 6 kg. The Lung Recruitment Tool provides an automated recruitment manoeuvre. Additional features include comprehensive pressure monitoring and customizable ventilatory support parameters.

Test lung: characteristics of the test lung compliance and simulated resistance; the test lung used had a compliance set at 0.5 L/cm$H_2O$ and a resistance of 20 mlbar/L – 500 mL, PEEP 0. – IMTMEDICAL Model –Light Lung – For Bellavista.

## 3. Experimental Protocol

Initial ventilator settings and test conditions included an inspiratory pressure (20 cm$H_2O$), PEEP (5 cm$H_2O$) and ventilation mode (Assist Control Mode - Pressure Control), fio2 was set to 50%., trigger sensitivity to 2 L, 12 RR/min, IE: 1:2.

Test Variant A: 10 ms – rise time

Test Variant B: 300 ms – rise time

Intervals and repeatability: The time interval for the mechanical work analysis of the test lung was set at every 6 seconds, repeated three times, at a room temperature of 21 °C.

The mechanical work of the test lung was analysed using a rise time setting of 10 ms, compared to the rise time setting of 300 ms. All other mechanical ventilation parameters were kept constant.

## 4. Measurements and calculation

The authors assess the concordance between the mechanical work values calculated by the ventilator and those derived from mathematical models, with the objective of optimizing ventilator settings to minimize pulmonary mechanical workload. This approach aims to mitigate the adverse effects associated with mechanical ventilation and represents a significant clinical challenge for intensivists in critical care settings.

Mathematical Calculation of the Natural Rise Time of Human Breathing:

Typical inspiratory-to-expiratory (I:E) ratio of 1:2, then:

$$\text{Tinspir} = \frac{Tcycle}{1+2}$$

On a standard breath At RR = 15 breaths/min

$$\text{Tcycle} = 60 \text{ seconds}/15 = 4\text{s}$$
$$\text{Tcycle} = 4\text{s Tinspiration} = \frac{4}{3} = 1333\text{ms}$$

After checking, we realized that there is a pattern of pressure plateau time of 800-950 ms (875 ms average), which indicates that at 1333 ms we have an average rise time of 400-458 ms: 1333ms – 875ms = 458ms (average time) rise time - Natural breathing

Pressure-Time Ramp Function

Assume a linear rise in pressure from 0 to the target pressure $P_{inspir}$ over the rise time $t_{riseP}$:

$$P(t) = \frac{Pinspir}{triseP} \times t \text{ for } 0 \le t \le trise$$
$$P_{insp} = 20 \text{ cm } H_2O$$
t-rise = either 0.01 s (10 ms) or 0.35 s (350 ms)

Flow Rate

Assuming constant compliance C, and V=C·P(t) then:

$$V(t) = \frac{dV}{vt} = C \times \frac{dP}{dt} = C \times \frac{Pinspir}{t\ rise}$$
C = 0.05 L/cmH2OC = 0.05

Then:

For 10 ms rise time:

THE ANNALS OF "DUNAREA DE JOS" UNIVERSITY OF GALATI
FASCICLE IX. METALLURGY AND MATERIALS SCIENCE
Nº. 1 - 2025, ISSN 2668-4748; e-ISSN 2668-4756
Article DOI: https://doi.org/10.35219/mms.2025.1.06

$$V = 0.05 \cdot \frac{20}{0.01} = 0.05 \cdot 2000 = 100 \text{ L/min}$$

For 350 ms rise time:

$$V = 0.05 \cdot \frac{20}{0.35} = 0.05 \cdot 57.14 = 2.85 \text{ L/min}$$

## 5. Experimental Validation

A test lung was connected to a mechanical ventilator, tests were performed at an inspiratory pressure of 20 $cmH_2O$ and PEEP of 5 cmH2O (Asist Control Mode-Pressure Control), using both low- and high-rise time values to determine effective pulmonary mechanical work.

Mechanical work was compared between two scenarios: one with fast rise time (10 ms) and the other with a slower rise time (300 ms), both conducted at an inspiratory pressure of 20 $cmH_2O$.

Mechanical work (W) during inspiration is broadly defined as:

$$W = \int P \cdot dV$$

P = pressure applied
V= volume delivered
Work = area under the pressure–volume curve
Rise Time 300 ms
$W2 \approx 10\ cmH_2O \times 0.5\ L = 5\ cmH_2O$ cdotpL x 0.098 = 0.49 J
Rise Time 10 ms
$W1 \approx 20\ cmH_2O \times 0.5\ L = 10\ cmH_2O$ cdotpL x 0.098 = 0.98 J

| **Rise Time** | **Mechanical Work ($cmH_2O \cdot L$)** | **Mechanical Work L(Joules)** | **Mechanical patient ventilator display software Delta L(J)** |
|---|---|---|---|
| 10 ms | 10 | 0.98 J | 0.99/0.94/0.97 |
| 300 ms | 5 | 0.49 J | 0.45/0.45/0.48 |

The last column displays the mechanical work values recorded by the mechanical ventilator for the virtual patient, with three consecutive measurements taken at 5-6 second intervals.

Preliminary results:

The shorter rise time (10 ms) results in greater mechanical work on the lungs, approximately double that observed with a rise time of 300 ms.

Higher Rise Time values (300 ms) lead to a considerable decrease in the mechanical work performed on the lungs, effectively halving the pressure exerted on them compared to a rise time of 10 ms.

## 6. Results and Discussion

This study emphasizes that a rise time setting of 10 milliseconds in mechanical ventilation results in a mechanically computed inspiratory work ranging from 0.099 to 0.94 joules per breath, as recorded by the ventilator's integrated software. These values were validated through comparison with mathematically derived calculations of mechanical work, underscoring the critical influence of rise time configuration on energy delivery to the respiratory system. Notably, when the rise time is adjusted to 300 milliseconds under otherwise identical ventilatory conditions, the mechanical work is reduced by approximately half. This finding highlights a fundamental consideration in ventilator management: the need for mandatory inclusion of adjustable rise time settings in all mechanical ventilators, and the prioritization of this feature by intensive care units to optimize lung-protective strategies and reduce ventilator-induced lung injury.

## 7. Conclusion

Clinical and Physiological Advantages of a 300 ms Rise Time in Mechanical Ventilation: A rise time setting of 300 milliseconds offers multiple clinical benefits by modulating the delivery of inspiratory pressure in a manner that closely approximates physiological breathing patterns. This intermediate rise time facilitates a more gradual pressure ramp, thereby avoiding abrupt pressure peaks that may be perceived as uncomfortable or unnatural by the patient. As a result, it enhances patient-ventilator synchrony and contributes to improved tolerance of ventilatory support. From a lung-protective standpoint, a slower rise in inspiratory pressure attenuates the initial flow rate and minimizes pressure overshoot, thereby reducing the risk of alveolar overdistension and ventilator-induced lung injury (VILI). Unlike shorter rise times (e.g., 50-100 ms), which can generate excessively high peak inspiratory flows and increase regional lung stress and strain, a 300 ms rise time promotes a more homogeneous distribution of tidal volume, which is especially advantageous in patients with heterogeneous lung mechanics, such as those with acute respiratory distress syndrome (ARDS). In pressure support ventilation, an excessively short rise time may lead to premature cycling or excessive pressure delivery, contributing to asynchrony. A rise time of 300 ms allows inspiratory pressure to reach the target level in closer alignment with the patient's inspiratory effort, thereby optimizing synchrony and potentially reducing the need for sedation. Moreover, this setting may reduce the dynamic mechanical work and mechanical power transmitted to the lungs with each breath. By distributing energy delivery more evenly, a 300 ms rise time may help mitigate the cumulative risk of ventilator-associated lung trauma over time.

## References

**[1]. Chiumello D., Pelosi P., Taccone P., Slutsky A., Gattinoni L.**, *Effect of different inspiratory rise time and cycling off criteria during pressure support ventilation in patients recovering from acute lung injury*, Crit Care Med., 31(11), p. 2604-10, doi: 10.1097/01.CCM.0000089939.11032.36. PMID: 14605531, Nov. 2003.

**[2]. Chiumello D., *et al.***, *Effect of different cycling-off criteria and positive end-expiratory pressure during pressure support ventilation in patients with chronic obstructive pulmonary disease*, Crit Care Med., 35(11), p. 2547-52, doi: 10.1097/01.CCM.0000287594.80110.34. PMID: 17893630, Nov. 2007.

**[3]. Kallet R. H., Corral W., Silverman H. J., Luce J. M.**, *Implementation of a low tidal volume ventilation protocol for patients with acute lung injury or acute respiratory distress syndrome*, Respir Care., 46(10):1024-37. PMID: 11572755, Oct. 2001.

**[4]. Simonis F. D., *et al.***, *Effect of a Low vs Intermediate Tidal Volume Strategy on Ventilator-Free Days in Intensive Care Unit Patients Without ARDS: A Randomized Clinical Trial*, JAMA, 320(18), p. 1872-1880, doi: 5.1001/jama.2018.14280. PMID: 30357256; PMCID: PMC6248136, Nov. 2018.

**[5]. Sison S. M., *et al.***, *Mortality outcomes of patients on chronic mechanical ventilation in different care settings: A systematic review*, Heliyon, 7(2):e06230, doi: 10.1016/j.heliyon.2021.e06230. Epub 2021 Feb 13. PMID: 33615014; PMCID: PMC7880845, Feb. 2021.

**[6]. Donahoe M. P.**, *Current venues of care and related costs for the chronically critically I*, ll. Respir. Care., 57(6), p. 867-888, doi: 10.4187/respcare.01656, 2012.

**[7]. Bhatraju P. K., Ghassemieh B. J., Nichols M.**, *Covid-19 in critically ill patients in the seattle region - case series*, N. Engl. J. Med., 382(21), p. 2012-2022, doi: 10.1056/NEJMoa2004500, 2020.

**[8]. Guan W. J., Ni Z. Y., Hu Y.**, *Clinical characteristics of coronavirus disease 2019 in China*, N. Engl. J. Med., 382(18), p. 1708-1720, doi: 10.1056/NEJMoa2002032, 2020.

**[9]. Wang D., Hu B., Hu C.**, *Clinical characteristics of 138 hospitalized patients with 2019 novel coronavirus-infected pneumonia in Wuhan, China*, JAMA, 323(11), p. 1061-1069, doi: 10.1001/jama.2020.1585, 2020.

**[10]. Yang X., Yu Y., Xu J.**, *Clinical course and outcomes of critically ill patients with SARS-CoV-2 pneumonia in Wuhan, China: a single-centered, retrospective, observational study*, [published correction appears in Lancet Respir Med. 2020 Apr;8(4):e26] Lancet Respir. Med., 8(5), p. 475-481, doi: 10.1016/S2213-2600(20)30079-5, 2020.

**[11]. McGrath B. A., Brenner M. J., Warrillow S. J.**, *Tracheostomy in the COVID-19 era: global and multidisciplinary guidance*, Lancet Respir. Med., 8(7), p. 717-725, doi: 10.1016/S2213-2600(20)30230-7, 2020.

THE ANNALS OF "DUNAREA DE JOS" UNIVERSITY OF GALATI
FASCICLE IX. METALLURGY AND MATERIALS SCIENCE
Nº. 1 - 2025, ISSN 2668-4748; e-ISSN 2668-4756
Article DOI: https://doi.org/10.35219/mms.2025.1.07

# EVALUATING THE SUSTAINABILITY OF MUNICIPAL WASTE MANAGEMENT IN ROMANIA

**Carmelia Mariana BĂLĂNICĂ DRAGOMIR, Marian Tiberiu COADĂ**
"Dunarea de Jos" University of Galati, Romania
e-mail: carmelia.dragomir@ugal.ro

## ABSTRACT

*The study examines the municipal waste generation per capita trends in Romania from 1995 to 2022 compared to other EU countries using Eurostat data. The analysis divides the period into two phases: pre-accession (1995-2008) and post-accession (2008-2022). In the first period, Romania maintained a low and stable waste generation rate, below 300 kg per capita per year, due to low consumption levels, incomplete waste collection, and limited waste management capacity. After joining the EU, there was a slight increase in waste generation, accompanied by improved data reporting and infrastructure, but Romania still had one of the lowest waste generation rates in the EU. Challenges remained in waste monitoring, rural collection, and public awareness. By contrasting Romania's data with high waste generating countries like Denmark and Germany, the study suggests that factors such as waste monitoring and public awareness contribute to lower waste per capita figures.*

KEYWORDS: waste management, recycling rate, waste generation, sustainable development, Romania

## 1. Introduction

Municipal waste generation serves as a key indicator of both consumption levels and the efficiency of waste management systems within a society. In the European context, the European Union closely monitors this metric, considering its environmental impact, as well as its relevance to circular economy and sustainability objectives [1].

Between 1995 and 2018, the average amount of municipal waste generated per capita in EU Member States consistently exceeded 500 kg per person per year.

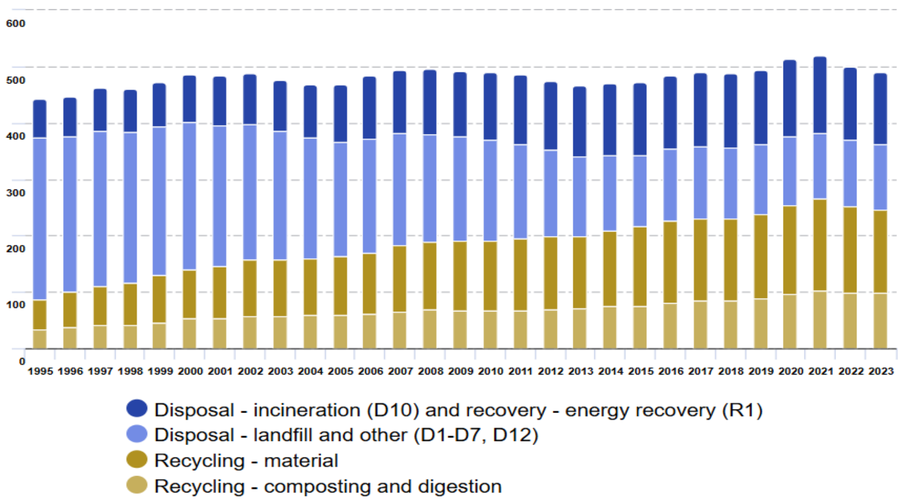


***Fig. 1.** Municipal waste treatment, 1995-2023 (kg/capita) Sourse Eurostat* [2]

THE ANNALS OF “DUNAREA DE JOS” UNIVERSITY OF GALATI
FASCICLE IX. METALLURGY AND MATERIALS SCIENCE
N°. 1 - 2025, ISSN 2668-4748; e-ISSN 2668-4756
Article DOI: https://doi.org/10.35219/mms.2025.1.07

Significantly higher values were recorded in countries such as Denmark, Germany, and Austria, where figures often surpassed 700–800 kg per capita [2].

In contrast, Romania has persistently ranked among the lowest in the EU, with reported averages below 300 kg per capita, according to official Eurostat data [2].

However, this seemingly favourable performance requires cautious interpretation. The low level of reported waste generation in Romania reflects, to a considerable extent, structural issues such as inadequate collection infrastructure—particularly in rural areas—systemic underreporting of actual waste quantities, and the prevalence of informal disposal practices [3].

Therefore, a comparative and context-sensitive analysis is essential to understand not only the quantity of municipal waste generated but also the underlying mechanisms behind its generation and management in Romania, in comparison with other European countries.

## 2. Methodology

The data analysed in this study are provided by Eurostat and published at the national level by the National Statistical Institute. The indicator ECC301A reflects the recycling rate of municipal waste, expressed in percentages, while ECC302A measures the amount of waste generated per capita in a calendar year, expressed in kilograms. Both datasets follow a standardized European methodology, ensuring comparability across countries and over time.

## 3. Results and discussion

### *3.1. Municipal waste recycling rate municipal*

Waste management has become a central element in the transition to a circular and sustainable economy, and the analysis of the two main indicators—the recycling rate and the amount of waste generated per capita—offers valuable insights into Romania's performance in this area [1].

The municipal waste recycling rate, defined as the proportion of the quantity of waste recycled to the total generated, reflects not only the efficiency of waste management infrastructure but also the level of public engagement. The targets set at the European level are ambitious: a recycling rate of 55% by 2025 and 60% by 2030 [2].

Romania, as a member state of the European Union, has committed to these goals, but available data suggest that progress remains insufficient. In many regions, material recycling is still limited, and composting or anaerobic digestion of biowaste is rarely implemented on a large scale [5].

One of the main obstacles to increasing the recycling rate is the lack of adequate infrastructure for separate collection, particularly in rural areas and disadvantaged communities. Additionally, the low level of environmental awareness and education among the population frequently leads to contamination of recycling streams, significantly reducing the efficiency of recycling process. Moreover, informal or non-compliant collection, alongside the absence of incentive systems for households, hinders the full potential of recycling in Romania [3].

The impact of recycling is not only ecological although this is the most visible aspect, as recycling contributes to pollution reduction, conservation of natural resources, and limitation of greenhouse gas emissions. However, the benefits are also economic and social: the development of the recycling sector can generate green jobs, encourage entrepreneurship, and strengthen the circular economy, while active citizen participation in collection and sorting fosters civic responsibility and community involvement [1].

### *3.2. Municipal waste generated per capita*

The amount of waste generated per capita is a key indicator of consumption behavior and the effectiveness of prevention measures. Although Romania records one of the lowest per capita figures in the EU, this value may be indicative of deficiencies in formal collection systems [2].

Changing consumption models, reducing packaging, and promoting reusable products are necessary solutions to decrease this indicator.

According to the hierarchy established by the Waste Framework Directive, waste prevention takes priority over recycling, reuse, or disposal [8].

Reducing the amount of waste produced per inhabitant is often seen as a sign of a society's ecological maturity. This involves not only technical or legislative measures but also a profound change in individual behavior: purchasing durable goods, avoiding unnecessary packaging, reusing products, and engaging in community waste reduction initiatives [6]. Furthermore, consumption models influenced by urban lifestyles or income growth can increase waste volumes in the absence of proactive policies for education and waste reduction.

It is important to note that Romania’s lower per capita waste figures, compared to the European average, may in some cases conceal issues such as under-reporting or informal collection.

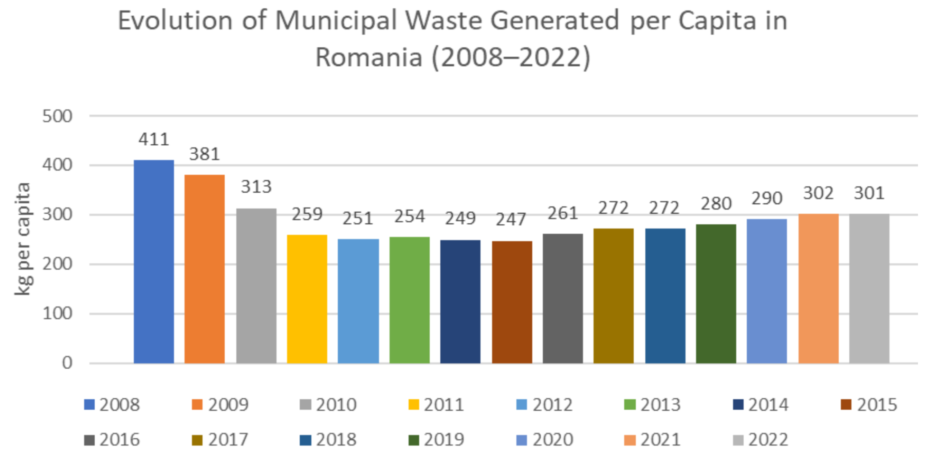


***Fig. 2.*** *Evolution of municipal waste generated per capita in Romania (2008–2022) (source: https://insse.ro/)* [4]

These situations, which exclude waste from the official statistical circuit, do not necessarily reflect better performance but rather gaps in monitoring and control systems [5].

### *3.3. Interdependence between indicators*

The interdependence between the two analysed indicators is particularly relevant: a smaller amount of waste generated facilitates efficient recycling, while a high recycling rate requires the existence of an effective collection and processing system. Together, these factors contribute to building a sustainable model of consumption and production where resources are maximized and environmental impact is minimized.

Between 2008 and 2021, Romania made significant progress in waste recycling, although not without challenges. In 2008, recycling was almost non-existent, with only 0.89% of waste managed through sustainable methods. In just a few years, notable progress was recorded.

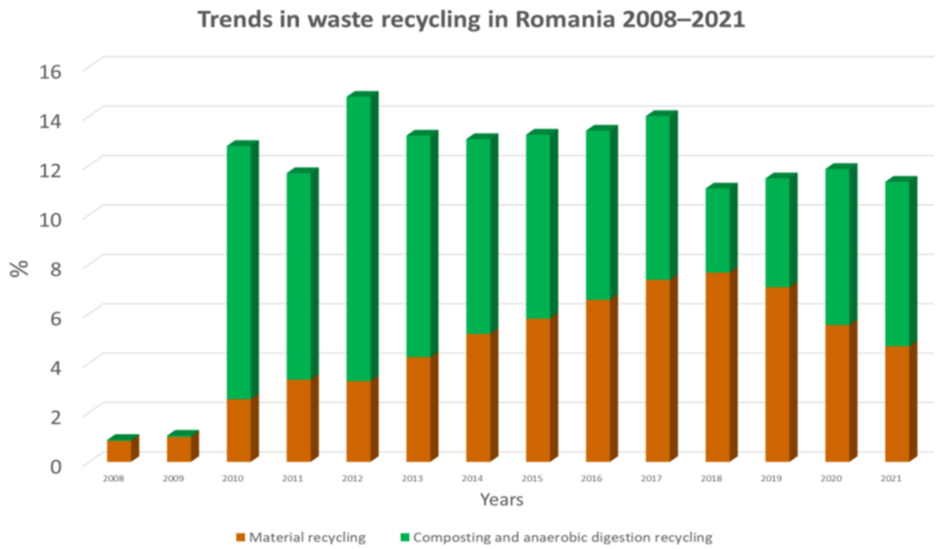


***Fig. 3.*** *Trends in waste recycling in Romania 2008–2021 (source: https://insse.ro/)* [4]

This period of growth was especially supported by the development of biowaste treatment through composting and anaerobic digestion. In 2010, this type of recycling surged from negligible values to over 10%, suggesting the emergence of new facilities and systems dedicated to organic waste.

At the same time, traditional material recycling—such as that of plastic, metal, or paper—increased more slowly but steadily, peaking in 2018 at 7.66%. This indicates that citizens and authorities began adapting to and adopting more sustainable habits, most likely following awareness campaigns and the introduction of separate collection systems in several cities [3].

However, after 2018, this positive trend reversed. The total recycling rate began to decline slightly, and material recycling experienced a more pronounced decrease. In 2021, only 4.68% of waste was recycled as material—a significant drop compared to previous years. At the same time, composting and anaerobic digestion fluctuated, suggesting a lack of a stable strategy for managing organic waste.

This stagnation and partial regression can be attributed to several factors: depletion of European funds, lack of continuity in public policies, inadequate infrastructure, and the 2020 health crisis, which disrupted waste collection and recycling services [5].

Romania's progress in recycling shows an encouraging initial phase followed, unfortunately, by a period of stagnation and decline. To ensure that these initial gains are not lost, it is essential to implement coherent public policies, secure long-term investment and strengthen institutional capacities dedicated to sustainable waste management.

## 4. Conclusions

The analysis of Romania's performance in municipal waste management between 2008 and 2021 reveals a complex and uneven trajectory. While notable progress has been made - particularly in the first years after EU accession - Romania continues to face structural and systemic challenges that prevent sustained improvement.

The recycling rate in Romania has seen a significant increase, particularly between 2008 and 2012, driven in part by the implementation of EU-aligned waste policies and an increased focus on the treatment of biodegradable waste through composting and anaerobic digestion. However, this upward trend did not persist after 2018, as both material recycling and processing of organic waste declined, suggesting a lack of long-term strategic planning and continued investment.

Romania reports one of the lowest municipal waste generation rates per capita in the European Union, but this is largely due to underdeveloped collection infrastructure and informal waste disposal practices rather than environmental efficiency. The interdependence between recycling rates and the amount of waste generated highlights the need for robust collection, separation and processing systems to facilitate efficient recycling. In Romania, limited recycling infrastructure and inconsistent implementation of separate waste streams have hindered the country's ability to maximize this synergy.

Moreover, public participation remains insufficient, reflecting gaps in environmental education, limited awareness, and insufficient economic incentives. A stronger civic engagement in waste sorting, reuse, and reduction efforts is essential for the transition to a more circular economy.

In conclusion, Romania’s current situation reflects a mix of initial policy-driven momentum and subsequent stagnation. In order to meet the EU’s recycling targets for 2025 and 2030, Romania must prioritize the expansion of separate collection systems, ensure transparency and accuracy in reporting, and invest in local waste treatment capacities. A shift from reactive to proactive strategies—anchored in education, infrastructure, and enforcement—is critical to transform short-term gains into long-term environmental stewardship.

## References

**[1]. European Commission**, *Circular Economy Action Plan*, https://environment.ec.europa.eu/strategy/circular-economy-action-plan_en, 2020.

**[2].** ***, *Municipal waste statistics*, https://ec.europa.eu/eurostat/statistics-explained/index.php/Municipal_waste_statistics, Eurostat, 2023.

**[3]. *****, *What a Waste 2.0: A Global Snapshot of Solid Waste Management to 2050*, World Bank, https://datatopics.worldbank.org/what-a-waste/, 2018.

**[4].** ***, National Institute of Statistics, INSSE, https://insse.ro/cms/.

**[5].** ***, *Waste management in Europe*, https://www.eea.europa.eu/en/analysis/indicators/waste-recycling-in-europe, European Environment Agency (EEA), 2024.

**[6].** ***, *Environment at a Glance*, https://www.oecd.org/environment/environment-at-a-glance/, OECD, 2022.

**[7]. *****, *Directive 2008/98/EC of the European Parliament and of the Council on waste*, https://eur-lex.europa.eu/legal-content/EN/TXT/?uri=CELEX%3A32008L0098.

THE ANNALS OF "DUNAREA DE JOS" UNIVERSITY OF GALATI
FASCICLE IX. METALLURGY AND MATERIALS SCIENCE
N°. 1 - 2025, ISSN 2668-4748; e-ISSN 2668-4756
Article DOI: https://doi.org/10.35219/mms.2025.1.08

# THE IMPACT OF PRESSURE ANGLE AND TOOTH ROOT ON THE MODIFIED ELLIPTICAL GEARS BENDING STRESS AND FATIGUE LIFE

**Paul-Adrian PASCU, Laurentia ANDREI**
"Dunarea de Jos" University of Galati, Romania
e-mail: paul.pascu@ugal.ro

## ABSTRACT

*Noncircular gears are receiving growing attention due to their ability to deliver variable transmission ratios and to optimize motions in specialized mechanical and industrial applications. Unlike circular gears, noncircular gears experience continuous variation in pressure angle and load distribution throughout the meshing cycle, leading to non-uniform stress states among teeth. This study explores the impact of pressure angle and tooth root radius on the bending stress and fatigue life of modified elliptical gears. Finite Element Analysis (FEA) is conducted on three representative teeth positioned at varying distances from the gear centre, highlighting the asymmetric loading characteristic of specific profiles. The tooth root radius is varied, showing a clear reduction in maximum stress with the increased fillet radius size. Then, by varying the rack cutter angle, it is shown that higher angles reduce stress concentration. The results reveal the critical influence of tooth position and geometry on the fatigue vulnerability in noncircular gear design.*

KEYWORDS: noncircular gears, bending stress, fatigue life

## 1. Introduction

Noncircular gears are mechanical components capable of transmitting rotary motion with a variable velocity ratio, offering unique advantages compared to traditional circular gears. Instead of having a constant radius, their shape follows a controlled variation that allows the gear to impose specific motion patterns during rotation. This property makes them particularly useful in specialized applications such as textile machinery with intermittent feeding cycles, variable-stroke pumps [1], moulding presses [2] with optimized force distribution, and robotic linkages [3] that require non-uniform angular velocities. Among noncircular geometries, elliptical gears are among the most widely used due to their relatively simple profiles and ease of integration into existing mechanisms.

Unlike circular gears, where each tooth is loaded under identical conditions, noncircular gears present a continuously changing loading scenario. Teeth stresses are affected by the pressure angle, contact point, and effective force arm throughout the rotation, which is determined by their position. Consequently, identifying the most critical tooth and understanding how design parameters affect stress levels are essential for reliable operation and fatigue performance.

In this paper, we analyse these two significant geometric parameters, the rack cutter pressure angle and the fillet radius at the tooth root, which are examined concerning the distribution of stress [4-6] during gear generation in modified elliptical gears. Using Finite Element Analysis (FEA), we analyse three distinct teeth located at different positions on the gear, as their loading conditions vary significantly due to the nonuniform geometry. The goal is to identify which tooth is subjected to the highest stress and how design adjustments can improve performance and reduce the risk of fatigue failure [7-9] in noncircular gear applications.

## 2. Gear design using the Gielis' supershape for the pitch curve

One of the key aspects in designing non-circular gears lies in defining the geometry of the driving gear's pitch curve. Given the virtually unlimited range of shapes that can be generated, along with the ease of adjusting a predefined contour, the Gielis

THE ANNALS OF "DUNAREA DE JOS" UNIVERSITY OF GALATI
FASCICLE IX. METALLURGY AND MATERIALS SCIENCE
Nº. 1 - 2025, ISSN 2668-4748; e-ISSN 2668-4756
Article DOI: https://doi.org/10.35219/mms.2025.1.08

superformula [10] is proposed as a suitable tool for describing the non-circular centrode. This equation offers a flexible parametric form capable of modeling a wide variety of closed curves, including modified elliptical shapes.

$$r_0(\varphi) = \left( \left| \frac{1}{a} \cos \frac{k\varphi}{4} \right|^{n_2} + \left| \frac{1}{b} \sin \frac{k\varphi}{4} \right|^{n_3} \right)^{-\frac{1}{n_1}} \tag{1}$$

where φ is the polar angle; $r_0$ - the polar coordinate of the "unit" centrode; *a, b* - the conventional ellipse semi-axes lengths, inscribed or circumscribed about the centrode; *k* – a real positive parameter that introduces the curve's rotational symmetry; $n_2$, $n_3$ – real positive parameters that lead to "polygonal" shapes; $n_1$ – a real positive and non-zero parameter that modifies the curve's geometry with respect to the linearity/convexity of the sides and the sharpness/flattening of the corners [11].

When the parameter *k* = 4, the superformula leads to modified elliptical shapes, suitable as gears pitch curves.

A fundamental parameter in gear design is the pressure angle, defined as the angle between the line of action and the common tangent to the pitch circles of two meshing gears. It is the parameter that determines the direction of force transmission of gear teeth during contact. A larger pressure angle will create a stronger tooth shape with greater load-carrying capacity, as it thickens the base of the tooth and reduce bending failure.

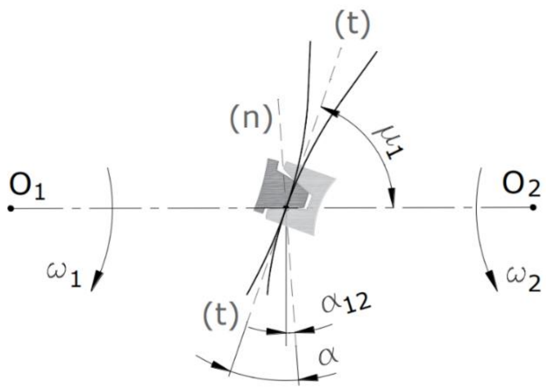


***Fig. 1.*** *Pressure angle components*

However, increasing the pressure angle also raises the radial component of the transmitted force, leading to higher bearing loads and potential vibration or noise issues. A smaller pressure angle improves smoothness and reduces friction but weakens the tooth root and increases stress concentration.

In noncircular gears, the pressure angle can vary dynamically during rotation, making it even more critical to control through design. Additionally, since the pressure angle is defined by the generating tool (such as the rack cutter), it directly influences the shape of the tooth flanks and the gear's mechanical performance.

The pressure angle is defined by equation:

$$\alpha_{12} = \mu \pm \alpha_c - \frac{\pi}{2} \tag{2}$$

$$\mu = \tan^{-1}\left(\frac{r_0(\varphi)}{r_0'(\varphi)}\right) \tag{3}$$

where $\alpha_c$ is the angle of the rack cutter, $r_0(\varphi)$ is the radius value at the contact point, and $r_0'(\varphi)$ is the derivate of the Gielis function.

In order to maintain the pressure angle within acceptable limits, Litvin [12] recommends limiting the pressure angle $\alpha_{12}$, which should remain within the range $-50° \leq \alpha_{12} \leq 50°$.

Exceeding the above range may result in unfavourable contact conditions and excessive lateral forces between the meshing teeth, which can compromise the smoothness and reliability of power transmission. Moreover, when a specific transmission ratio is required, it is often nearly impossible to adjust the pressure angle directly, since the geometry of the pitch curve is already constrained. In such instances, the optimal solution is to alter the generating tool angle ($\alpha_c$).

Based on the theoretical considerations presented above, a specific case study was developed using the Gielis superformula to define the pitch curve geometry of the driving gear. The noncircular centrode was designed using the following parameters: *a = 1.3*, *b = 1*, *k = 4*, $n_1 = 2.5$, $n_2 = 2.5$,

THE ANNALS OF “DUNAREA DE JOS” UNIVERSITY OF GALATI
FASCICLE IX. METALLURGY AND MATERIALS SCIENCE
N°. 1 - 2025, ISSN 2668-4748; e-ISSN 2668-4756
Article DOI: https://doi.org/10.35219/mms.2025.1.08

$n_3 = 2$. The “unit centrode” was further scaled to fit as the gear pitch curve, choosing 28 teeth and a module of 1 mm for the gear geometry; the addendum and dedendum were set to standard values of 1 mm and 1.25 mm, respectively, ensuring proper tooth engagement and clearance. The gear face width was set to 3 mm. Prior to conducting the finite element simulations, the variation of the pressure angle along the generated pitch curve was examined to ensure that all values remained within the range recommended by Litvin. The variation is presented in Fig. 2 considering an initial $\alpha_c$ = 20°. This validation step was essential to confirm the feasibility of the selected noncircular profile.

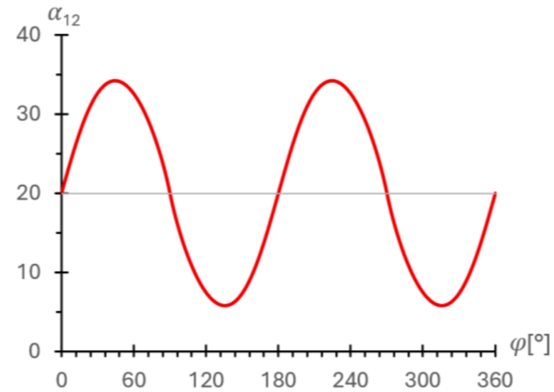


***Fig. 2.*** *Variation of pressure angle*

The noncircular gear was generated using the enveloping theory [13], where the tooth profile results from the envelope of a single rack cutter tooth moving in pure rolling motion along the pitch curve. For the generation of the analysed cases, three rack cutters were used, each with a different pressure angle: 18°, 20°, and 22° (Figure 3). These values were chosen to investigate how the tool geometry influences the resulting tooth profile and the stress distribution in the gear. The generation of the tooth profile using a 20° rack cutter is shown in Figure 4.

The gear generation was simulated in AutoCAD using an AutoLISP code. To reduce the number of elements during finite element analysis, only a segment of the driving and driven gears was modeled.

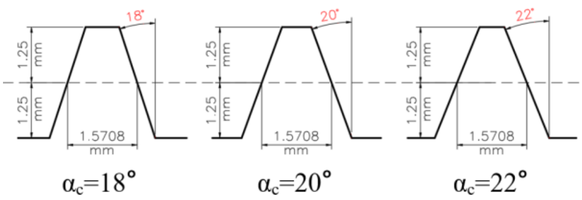


Fig. 3. Rack cutter design

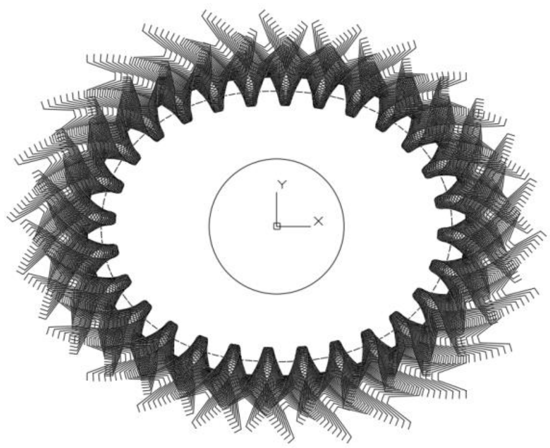


***Fig. 4.*** *Tooth profile generation using the enveloping theory*

Three teeth were selected in key positions along the pitch curve to be analysed in detail. Figure 5 shows the selected contact points along with the angles at which contact takes place.

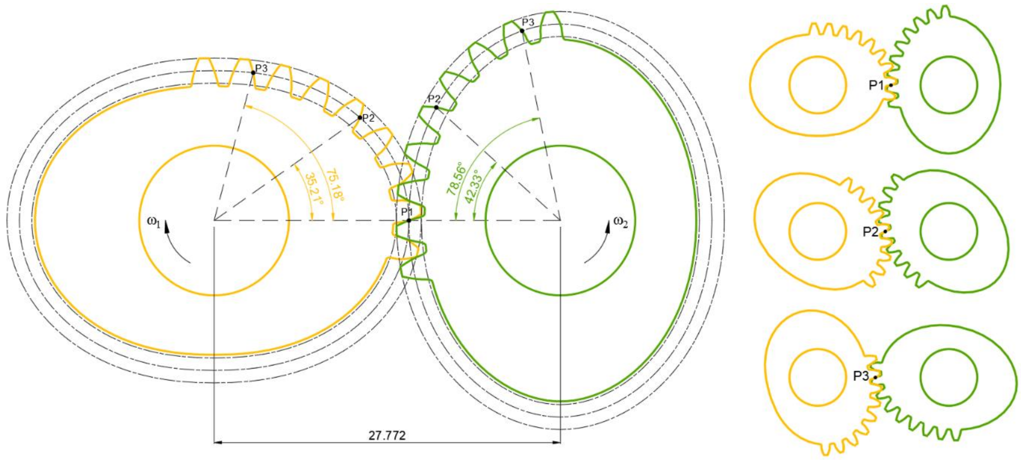


***Fig. 5.*** *Segments of generated gears and selected contact points during meshing*

THE ANNALS OF "DUNAREA DE JOS" UNIVERSITY OF GALATI
FASCICLE IX. METALLURGY AND MATERIALS SCIENCE
N°. 1 - 2025, ISSN 2668-4748; e-ISSN 2668-4756
Article DOI: https://doi.org/10.35219/mms.2025.1.08

The tooth root fillet radius obtained through the enveloping theory is approximately 0.15 mm. However, with the advent of modern manufacturing technologies such as EDM and CNC machining, the enveloping theory often serves only as a virtual tool for gear profile generation. In practice, the obtained tooth shape can also be optimized or adjusted after preliminary profile synthesis.

For this reason, another objective of the study was to investigate the potential reduction of bending stress by increasing the root fillet radius. Simulations were also performed for enlarged radii of 0.20 mm and 0.25 mm (Figure 6), allowing the evaluation of how root geometry modifications affect stress concentration and fatigue resistance.

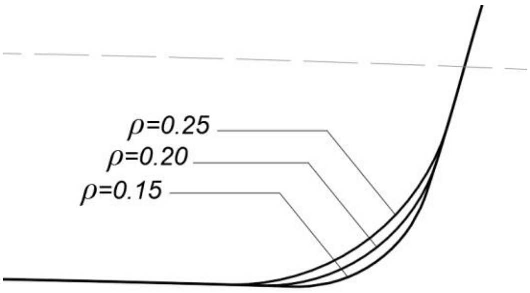


***Fig. 6.*** *Variation of the tooth root fillet radius*

After the geometry was finalized, the model was exported to Ansys and prepared for finite element analysis. A coarse mesh was applied globally, with local refinement in two critical areas: the contact zone and the tooth root region, where bending stresses are expected to be highest. In these regions, the element size was set to 0.05 mm, resulting in a total of approximately 33,000 elements and 42,000 nodes, with slight variations depending on the analysed case.

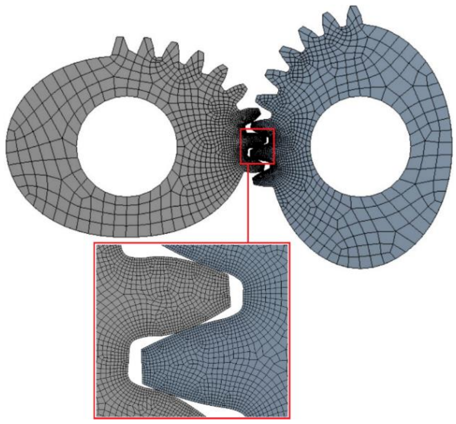

***Fig. 7.*** *Mesh discretization*

The driven gear was fully constrained, while a torque of 2,000 Nmm was applied to the driving gear to simulate loading conditions.

## 3. Results and discussions

Three teeth were chosen in different areas of the gear to be analysed individually. The results are grouped based on the root radius (0.15 mm, 0.20 mm, 0.25 mm) and cutter angles (18°, 20°, 22°), so that we can easily compare how each change influences stress levels. For each case, the maximum stress value at the tooth base was recorded.

First, a total of nine simulations were carried out, three for each selected contact point. In each case, the tooth root fillet radius was varied between 0.15 mm, 0.20 mm, and 0.25 mm to observe how this parameter influences the bending stress at the base of the tooth. The results for the first case, where the rack cutter angle is 20° and the tooth root fillet radius is 0.15 mm, are shown in Figure 8. The stress distribution is presented for all three contact points, both on the driving gear and the driven gear.

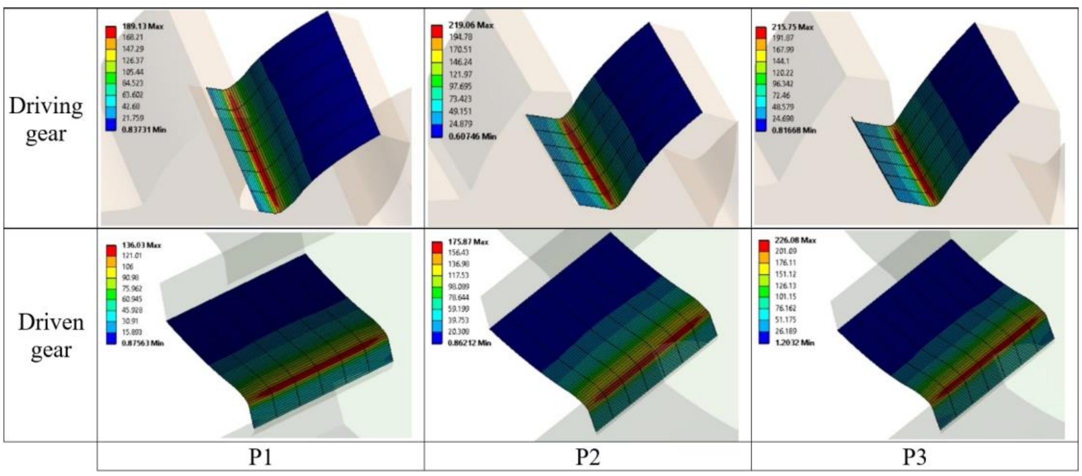


***Fig. 8.*** *Von-Mises stress on the tooth root, αc = 20°, ρ = 0.15 mm*

N°. 1 - 2025, ISSN 2668-4748; e-ISSN 2668-4756
Article DOI: https://doi.org/10.35219/mms.2025.1.08

The remaining results for αc = 20°, with root radii of 0.20 mm and 0.25 mm, are shown in Figures 9 and 10, for the driving gear and driven gear, respectively, allowing for a direct comparison between the two. The chart displays the maximum von Mises stress values at all three contact points (P1, P2, and P3) and all radii values.

For the driving gear (Figure 9), the highest stress levels occur at P2, closely followed by P3, with maximum values reaching 219.06 MPa and 215.75 MPa, respectively, when ρ = 0.15 mm. As the root radius increases to 0.25 mm, the stress at these points drops by 13.46%, confirming the effectiveness of fillet radius optimization in reducing bending loads.

For the driven gear (Figure 10), a similar trend is observed. The highest value appears at P3, with a maximum of 226.08 MPa for the smallest radius. Again, increasing ρ decreases the stress significantly, with a reduction of 9.69% at ρ = 0.25 mm.

These results show that the critical tooth position on the driven gear is P3.

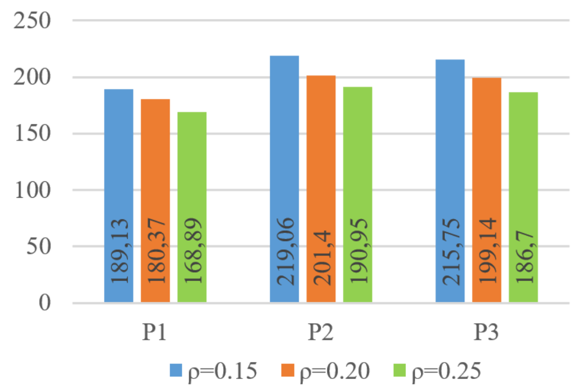


***Fig. 9.** Maximum von Mises Stress at Tooth Root – Driving Gear*

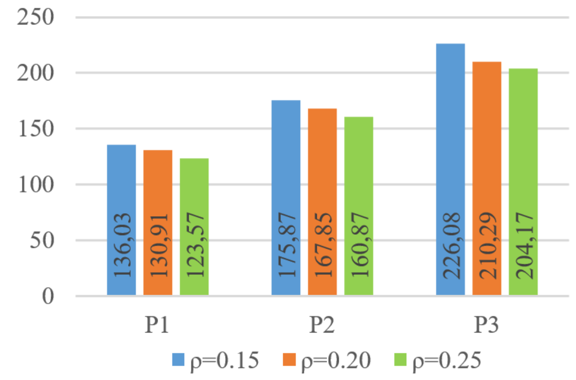


***Fig. 10.** Maximum von Mises Stress at Tooth Root – Driven Gear*

After identifying that the lowest stress values occurred for a root fillet radius of 0.25 mm, a second set of simulations was performed to study the influence of the rack cutter pressure angle (αc). New gear geometries were generated using αc = 18° and 22°.

The results of these simulations are shown in Figure 11 and Figure 12, where the maximum von Mises stress at the tooth root is compared for all three contact points (P1, P2, and P3), both on the driving and the driven gear. Reducing the rack cutter angle to 18° resulted in an increase in stress values of up to 5%, while increasing the angle to 22° led to a reduction in stress of up to 7% compared to the original case at 20°. This confirms the positive effect of using a slightly larger pressure angle on bending stress reduction, due to the increased thickness at the tooth root.

Overall, the results indicate that both tooth root radius and the rack cutter angle play a crucial role in determining stress concentration at the tooth's base. While the direct impact of radius is clear, an impact on pressure angle can also lead to a notable improvement in gear strength.

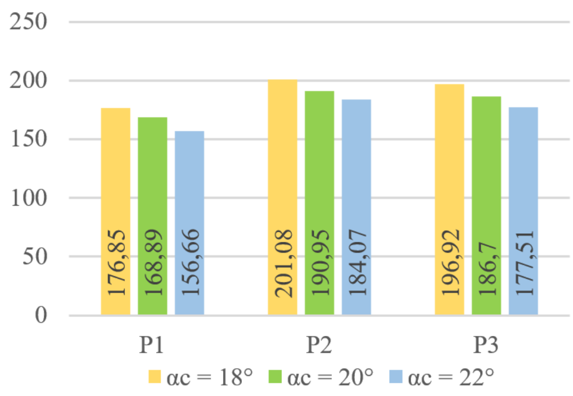


***Fig. 11.** Maximum von Mises Stress at Tooth Root – Driving Gear*

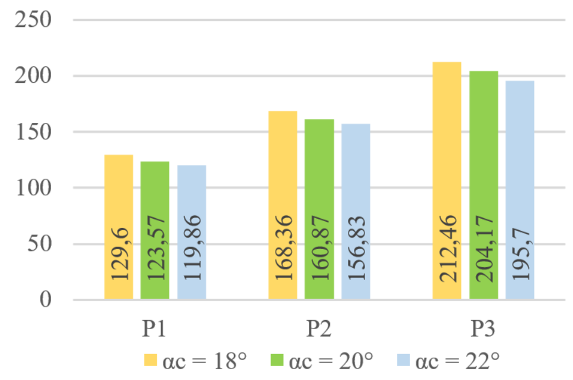


***Fig. 12.** Maximum von Mises Stress at Tooth Root – Driven Gear*

Since gear teeth are typically subjected to repeated cyclic loading during operation, evaluating fatigue behavior is essential for predicting long-term

N°. 1 - 2025, ISSN 2668-4748; e-ISSN 2668-4756
Article DOI: https://doi.org/10.35219/mms.2025.1.08

durability and avoiding premature failure. Crack formation can occur over time due to localized stress concentrations at the tooth root, even if the static stress levels remain below the material's yield strength. For this reason, the next step in the study focuses on analysing the potential for fatigue failure.

The number of load cycles was calculated for each gear based on the applied torque during rotation. This analysis was carried out for three different configurations, corresponding to rack cutter pressure angles of 18°, 20°, and 25°, to observe how tooth geometry influences fatigue life. The results are presented in Figure 13. The focus was on identifying the variation in expected life between the driving and driven gears for each case. For a given torque level, the gear generated with $\alpha c = 22°$ consistently supports a higher number of cycles compared to the other configurations. In contrast, the geometry with $\alpha c = 18°$ exhibits the shortest fatigue life at all load levels.

This confirms that a larger pressure angle not only reduces bending stress but also enhances fatigue resistance, likely due to the thicker tooth root and lower stress concentration.

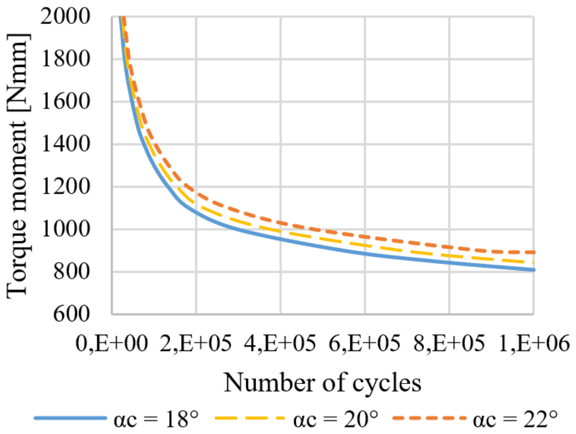


***Fig. 12.*** *Fatigue Life Curves*

For example, at a torque of 1000 Nmm, the fatigue life increases by approximately 58% when the pressure angle is increased from 18° to 22°, rising from $2.98 \times 10^5$ to $4.73 \times 10^5$ cycles. In general, fatigue life increases by between 30% and 60% across the two extreme cases analysed ($\alpha c = 18°$, $\alpha c = 22°$), highlighting the significant influence of the rack cutter angle on the gear’s durability.

## 4. Conclusions

The results of this study confirm that both the tooth root fillet radius and the rack cutter pressure angle have a significant impact on the stress distribution and fatigue life of modified elliptical gears. Increasing the root radius consistently results in a decrease in bending stress while improving fatigue resistance, particularly at the most heavily loaded tooth positions.

However, when designing noncircular gears, one must also consider the geometric constraints imposed by the pitch curve. In some cases, it may be necessary to reduce the pressure angle to keep it within the limits recommended by Litvin (±50). While this adjustment guarantees proper meshing, it often results in higher stress levels and reduced fatigue life.

On the other hand, a higher rack cutter angle can be effective in minimizing bending stress and maximizing gear life. Yet, this approach has its own drawbacks, as it tends to increase the radial force component, which may result in increased vibrations and noise, as well as increasing bearing loads.

Both low- and high-pressure angles have their advantages and disadvantages. The optimal solution depends on the specific application, design constraints, and performance requirements. A balanced approach is required to ensure both mechanical strength and smooth operation in real-world conditions.

## References

**[1]. Zeng Q., Sun J.**, *Analysis of flow of outer meshing elliptic gear pump based on Fluent*, International Conference on Advanced Electronic Science and Technology, 2016.

**[2]. Yokoyama T.**, *Powder modeling press*, United States of America Brevet 5547360A, 20 August 1996.

**[3]. Huang K.-J., Chen S.-C., Tsai M.-C., *et al.***, *A Bio-inspired Hexapod Robot with Noncircular Gear Transmission System*, IEEE/ASME International Conference on Advanced Intelligent Mechatronics, Kaohsiung, Taiwan, 2012.

**[4]. Pedersen N. L.**, *Improving bending stress in spur gears using asymmetric gears and shape optimization. Mechanism and machine theory*, 45 (11), p. 1707-1720, 2010.

**[5]. Rathore R. K., Tiwari A.**, *Bending Stress Analysis & Optimization of Spur Gear*, International Journal of Engineering Research, 3(5), 4, 2014.

**[6]. Kyung-Eun K. O., *et al.***, *A study on the bending stress of the hollow sun gear in a planetary gear train*, Journal of mechanical science and technology, 24, p. 29-32, 2010.

**[7]. Rey G., González, Martín R. G., Fernández P. Frechilla**, *Estimating gear fatigue life*, Gear Solutions, 2.6, 2007.

**[8]. Olsson Erik, Olander Anton, Öberg Martin**, *Fatigue of gears in the finite life regime—Experiments and probabilistic modelling*, Engineering failure analysis, 62, p. 276-286, 2016.

**[9]. Mao K.**, *Gear tooth contact analysis and its application in the reduction of fatigue wear*, Wear, 262, 11-12, p. 1281-1288, 2007.

**[10]. Gielis J.**, *Method and apparatus for synthesizing patterns*, Europe Brevet, EP 1177529 B1, 10 Mai 2000.

**[11]. Pascu P.-A., Andrei L.**, *Gielis’transformation as Potential Application for Convex Bilobe Centrodes*, 2023.

**[12]. Litvin F. L., *et al.***, *Noncircular Gears. Design and generation*, New York: Cambridge University Press, 2009.

**[13]. Litvin Faydor L., Fuentes Alfonso**, *Gear geometry and applied theory*, Cambridge university press, 2004.

MANUSCRISELE, CĂRŢILE ŞI REVISTELE PENTRU SCHIMB, PRECUM ŞI ORICE CORESPONDENŢE SE VOR TRIMITE PE ADRESA:

MANUSCRIPTS, REVIEWS AND BOOKS FOR EXCHANGE COOPERATION, AS WELL AS ANY CORRESPONDANCE WILL BE MAILED TO:

LES MANUSCRIPTS, LES REVUES ET LES LIVRES POUR L'ECHANGE, TOUT AUSSI QUE LA CORRESPONDANCE SERONT ENVOYES A L'ADRESSE:

MANUSCKRIPTEN, ZIETSCHRITFTEN UND BUCHER FUR AUSTAUCH SOWIE DIE KORRESPONDENZ SID AN FOLGENDE ANSCHRIFT ZU SEDEN:

After the latest evaluation of the journals by the National Center for Science Policy and Scientometrics (**CENAPOSS**), in recognition of its quality and impact at national level, the journal will be included in the $B^+$ category, 215 code (http://cncsis.gov.ro/userfiles/file/CENAPOSS/Bplus_2011.pdf).

The journal is already indexed in:

DOAJ: https://doaj.org/

SCIPIO-RO: http://www.scipio.ro/web/182206

EBSCO: http://www.ebscohost.com/titleLists/a9h-journals.pdf

Google Academic: https://scholar.google.ro

Index Copernicus: https://journals.indexcopernicus.com

Crossref: https://search.crossref.org/

The papers published in this journal can be viewed on the website: http://www.gup.ugal.ro/ugaljournals/index.php/mms

**Name and Address of Publisher:**
Contact person: Prof. Dr. Eng. Elena MEREUȚĂ
Galati University Press - GUP
47 Domneasca St., 800008 - Galati, Romania
Phone: +40 336 130139
Fax: +40 236 461353
Email: gup@ugal.ro

**Name and Address of Editor:**
Ș. L. Dr. Eng. Marius BODOR
"Dunarea de Jos" University of Galati, Faculty of Engineering
111 Domneasca St., 800201 - Galati, Romania
Phone: +40 336 130208
Phone/Fax: +40 336 130283
Email: marius.bodor@ugal.ro

**AFFILIATED WITH:**

- **THE ROMANIAN SOCIETY FOR METALLURGY**
- **THE ROMANIAN SOCIETY FOR CHEMISTRY**
- **THE ROMANIAN SOCIETY FOR BIOMATERIALS**
- **THE ROMANIAN TECHNICAL FOUNDRY SOCIETY**
- **THE MATERIALS INFORMATION SOCIETY (ASM INTERNATIONAL)**

**Edited under the care of**
**the FACULTY OF ENGINEERING**
**Annual subscription (4 issues per year)**

Fascicle DOI: https://doi.org/10.35219/mms

Volume DOI: https://doi.org/10.35219/mms.2025.1

Editing date: 15.03.2025
Number of issues: 200
Printed by Galati University Press (accredited by CNCSIS)
47 Domneasca Street, 800008, Galati, Romania